Photochemical Production of Ozone and Emissions of NO$_x$ and CH$_4$ in the San Joaquin Valley

Justin F. Trousdell[1], Dani Caputi[1], Jeanelle Smoot[2], Stephen A. Conley[3], Ian C. Faloona[1]

[1]Department of Land, Air, and Water Resources, University of California Davis, United States
5 [2]Department of Chemistry, University of California Davis, United States
[3]Scientific Aviation, Inc., Boulder, Colorado, United States

Correspondence to: Ian C. Faloona (icfaloona@ucdavis.edu)

Abstract. Midday summertime flight data collected in the atmospheric boundary layer (ABL) of California's San Joaquin Valley (SJV) are used to investigate the scalar budgets of NO$_x$, O$_3$, and CH$_4$ in order to quantify the individual processes that
10 control near surface concentrations yet are difficult to constrain from surface measurements alone: these include most importantly, horizontal advection and entrainment mixing from above. The setting is a large mountain-valley system with a small aspect ratio where topography and persistent temperature inversions impose strong restraints on ABL ventilation. In conjunction with the observed time rates of change this airborne budgeting technique enables us to deduce net photochemical ozone production rates and emission fluxes of NO$_x$ and CH$_4$. Estimated NO$_x$ emissions from our principal flight domain
15 averaged 216 ($\pm$ 33) metric tons per day over six flights in July and August, which is nearly double the California government's NO$_x$ inventory for the surrounding three county region. We consider several possibilities for this discrepancy including the influence of wildfires, the temporal bias of the airborne sampling, instrumental interferences, and the recent hypothesis presented by Almaraz et al. (2018) of localized high soil NO emissions from intensive agricultural application of nitrogen fertilizers in the region and find the latter to be the most likely explanation. The methane emission average was 438 Gigagrams
20 per year ($\pm$ 143), which exceeds an emissions inventory for the region by almost a factor of two as well. Measured ABL ozone during the six afternoon flights averaged 74 ppb (σ=9.8 ppb). The average mid-afternoon ozone rise of 2.8 ppb h^{-1} was found to be comprised of -0.8 ppb h^{-1} due to horizontal advection of lower O$_3$ levels upwind, -2.5 ppb h^{-1} from dry deposition loss, -0.5 ppb h^{-1} from dilution by entrainment mixing, and 6.9 ppb h^{-1} net in-situ photochemical production. The O$_3$ production rates exhibited a dependence on NO$_2$ concentrations (r^2 = 0.35), and no discernible dependence on methane concentrations (r^2 ~
25 0.02) which are correlated with many of the dominant VOC's in the region, suggesting that the ozone chemistry was

predominantly NOₓ-limited on the flight days. Additionally, in order to determine the heterogeneity of the different scalars, autocorrelation lengths were calculated for potential temperature (18 km), water vapour (18 km), ozone (30 km), methane (27 km), and NO_x (28 km). The spatially diffuse patterns of CH_4 and NO_x seem to imply a preponderance of broad areal sources rather than localized emissions from cities and/or highway traffic within the SJV.

1 Introduction

The setting for this research is the San Joaquin Valley (SJV) (see Figure 1) which is the southern end of California's Central Valley, one of the largest valleys by area in the world. The SJV is a complex mesoscale environment where the surrounding topography limits the low-level inflow to the valley and renders vertical mixing of particular importance to atmospheric boundary layer (ABL) ventilation, similar to conditions in the Po Valley of Italy (Maurizi et al., 2013). Estimates of the coverage of mountainous terrain on the Earth's land surface varies anywhere from ~25% − 70% (Grab, 2000; Noppel and Fiedler, 2002; Rotach et al., 2014), depending on the subjective criterion used, and thus orographically-induced mesoscale circulations are of paramount importance in understanding the earth-atmosphere exchange (EAE) over much of the continental land area. Horizontal inhomogeneities in the Earth's land surface affect the adjacent ABL in a variety of ways leading to pronounced changes in the EAE involving sea-breezes (Miller et al., 2003), internal boundary layers (Garratt, 1990), and orographic effects (Rotach et al., 2015). Additionally, valleys are popular areas for human inhabitation due to lowland access, access to river waterways, and fertile soils for agriculture (Christopher Small and Joel E. Cohen, 2004).

The SJV is well known for its persistent air quality challenges (Lagarias & Sylte, 1991; Cox et al., 2013). As of 2013 the Valley is a non-attainment site for the state (California Air Resources Board (CARB)) and federal 8-hour standard for O_3, a status that is only aggravated by the recent reduction in the federal 8h standard to 70 ppbv (US EPA). Moreover, the majority of the SJV, especially its southern end, has been designated non-attainment for PM2.5 for the state and federal standards since 2013. The need to understand and find solutions to these air quality issues has been the catalyst of numerous studies, including major multi-researcher field campaigns. In 1990, the San Joaquin Valley Air Quality Study (SJVAQS) was conducted. The largest study of its kind in the U.S. at the time, the SJVAQS targeted the complexities of the SJV at a time when it was considered the nation's second worst overall air quality problem (Lagarias and Sylte, 1991). In 2000, the Central California

Ozone Study (CCOS), a multi-year program of meteorological and air quality monitoring, emission inventory development, and air quality simulation modelling, held its intensive observation period. And in 2010 the California Research at the Nexus of Air Quality and Climate Change Study (CALNEX) (Ryerson et al., 2013) was conducted across Southern California and the SJV. These traditional studies tended to focus on ground-based atmospheric chemistry observations in the SJV measuring

5   as many different components of the oxidation chemical mechanism as possible in one location, for example at a "supersite" in Fresno, CA (Watson et al., 2000). However, a prominent meteorological process that can strongly influence surface concentrations is mesoscale advection by the horizontal flow, and due to the complexity of the surface wind field in complex terrain and the heterogeneity of surface sources this process's contribution to local air quality problems is difficult to account for in these types of studies. Furthermore, in studies that do deploy airborne platforms, the flight data tend to be limited in

10   duration or overextended in sampling domain and/or altogether uncoordinated with the surface sites, never attempting to measure advection quantitatively.

Another essential process influencing air quality at surface sites is mixing at the top of the ABL, or entrainment. Entrainment, the dynamical process whereby a turbulent mixed layer incorporates adjacent fluid that is laminar or much less turbulent, predominantly drives the daytime ABL growth, and is generally a diluting process when considering trace gases with surface

15   sources (or precursors.) Local ABL air affected by surface emissions is diluted with background, less-turbulent, and typically warmer and dryer air in which pollutant concentrations remain relatively low (Stull, 1988). This classical image is complicated, however, when polluted air is transported locally, regionally, and/or synoptically to the free atmosphere above the ABL before being entrained, which is often the case in mountainous terrain.

Wheeler et al. (2010) investigated ozone events that occurred during CCOS and found that the tendency of photochemical

20   models to underestimate peak ozone was likely due to an under-representation of emissions, particularly from wildfires, as well as regional recirculation and transport of ozone and/or ozone precursors aloft across the model's boundaries. Polluted ABL air can also be vertically recirculated in complex terrain by slope venting along valley sidewalls only to be reincorporated into the valley boundary layer via entrainment (Fast et al., 2012;Leukauf et al., 2016;Henne et al., 2004). Moreover, a growing body of evidence is suggesting that distal air pollution can represent a significant source of local air quality degradation in the

Western U.S. as a result of entraining air masses that have been transported across the Pacific (Parrish et al., 2010; Huang et al., 2010; Lin et al., 2012; Pfister et al., 2011; Ewing et al., 2010).

In addition to issues of long-range transport, mesoscale dynamics, and turbulent mixing there are outstanding questions about the chemistry and sources of pollutants in the SJV. Pusede and Cohen (2012) suggested the existence of a temperature-dependent VOC in the SJV and their results indicated that the trend in ozone exceedance days, at least over the past dozen years or so, was due to a transition to NO_x-limited photochemistry and ongoing NO_x reduction strategies in the region. Even with a well-accepted theory of ozone chemistry, discrepancies still exist between measured and modelled ozone from regional air quality models (Brune et al., 2016). That study found ozone production rates from HO_2 around the morning rush hour to be double modelled rates when NO typically reached its highest diurnal levels, and measured HO_2 in instances of the very highest observed NO was seen to rise to more than ten times the modelled values. Another study from the same CalNex surface data set posited that an unknown temperature-dependent VOC, quite possibly of agricultural origins, dominates OH reactivity at high temperatures when O_3 problems are most likely (Pusede et al., 2014). Agricultural sources of NO_x, an important precursor for ozone production and a dangerous pollutant in and of itself, were estimated using three independent methods in the study of Almaraz et al. (2018) suggesting that California's croplands may account for 20-51% of the state's overall NO_x emissions while current CARB inventories assume that the contribution from soils is insignificant.

The purpose of this study is to employ in-situ aircraft data, including meteorological and chemical data, collected predominately during the summer of 2016 in the SJV for an integrated study of ozone, NO_x, and methane employing a scalar budget technique. The individual terms of the scalar budgets, which are responsible for the observed overall time rates of change in the ABL, are calculated enabling a relative comparison of each individual process. This method includes treatments of both horizontal advection and entrainment mixing – essential processes not well captured in modelling or ground-site studies.

2 Geophysical Setting and The Buffer Layer

In the southern SJV prevailing northwesterly surface winds (parallel with the valley axis) slow down as they converge against a topographical cul-de-sac leading to stagnation. The SJV has a long and deep geography, running approximately 400 km

(Stockton to Arvin) bounded at over 3 km on its northeastern flank (Southern Sierra Nevada), ~1 km to its southwest (Diablo and Temblor Ranges), and ~2 km at its terminus (San Emigdio and Tehachapi Mountains, see Figure 1). The surface airflow in the SJV comes through gaps and cols in the Pacific Coast Range, predominately around the San Francisco Bay Area and through the Carquinez Strait bringing fresh emissions of NO_x and VOC precursors from those urban areas. These precursors

5 generate ozone concentrations that typically increase as the air mass moves southeast, often reaching a maximum in the southern end of the valley near Bakersfield (Cox, 2013). This north to south gradient can be seen in Figure 2 from four observation stations in the SJV showing the annual pattern of the probability of ozone exceedances from 10 years of CARB data spanning 2006 to 2015. However, the horizontal distribution of ozone is not always so straightforward and different 'background' meteorological conditions have been shown to distort this general pattern (Jin et al., 2011).

10 Elevated temperature inversions above the SJV in the summer, which are present almost every day of the year (Iacobellis et al., 2009), constrain vertical air motions and impede the venting of air pollution. These inversions, coupled with the topographic isolation of the SJV air along the valley floor, make the valley's air quality strongly dependent not only on local emissions but also on the nature of the entrainment mixing. The air above the ABL in the SJV is unique in that it does not purely consist of background air from the free troposphere (FT) as in most cases over flat terrain. A three-layer conceptual system has been

15 presented in Faloona et al. (2019) for the SJV comprised of: the ABL, a buffer layer, and the FT. This buffer layer is an admixture of 'background' air masses aloft (FT) that flow over the Coast Range mountains, with a Froude number of order 0.1, and stagnate against the Sierra Nevada Mountains, mixed with SJV boundary layer air that is transported vertically along the valley sidewalls on its transit up the valley. The vertical extent of the buffer layer begins atop the ABL, which across the region in the afternoons during the summer average around 600 m, up to roughly 2000 m (AGL). The approximate residence time

20 within this buffer layer was found to be about one week based on analysis of WRF model output which we plan to detail in a forthcoming paper.

3 Methods

3.1 WRF Model Configuration

The Weather Research and Forecasting (WRF) model version 3.8.1 was used in hindcast to provide vertical velocities essential to the study but not measured by the aircraft. The model was configured using two, two-way nested domains initialized at 12 and 4-kilometer resolution. Much of the coarser domain covers the Western United States, while the finer resolution domain is centred around California and Nevada. This model configuration features fifty terrain following vertical levels, with thirty levels being located below five kilometres in height, and an increased resolution near boundary layer heights within the SJV. The Moderate Resolution Imaging Spectroradiometer (MODIS) dataset was used for land usage categories. The North American Regional Reanalysis (NARR) data set was used to initialize model runs, and new initial conditions were introduced every 3 hours. In addition, four-dimensional data assimilation (FDDA) was utilized in the coarse domain for wind speeds in every vertical level, and temperature/water vapour within the lowest vertical level and above the planetary boundary layer. FDDA used the National Centres for Environmental Prediction (NCEP) Administrative Data Processing (ADP) Global Surface Observational Weather Data (ds461.0) and Upper Air Observational Weather Data (ds351.0), both of which are at 6-hour temporal resolution, to nudge model runs.

3.2 Aircraft Instrumentation

Aircraft data were collected by a Mooney Bravo and Mooney Ovation, which are fixed-wing single engine airplanes operated by Scientific Aviation, Inc. The wings are modified to sample air through inlets under the starboard wing that draw air to the on-board analysers through 3.18 mm (outer diameter) stainless steel (for CH_4, CO_2, and H_2O), and 6.35 mm PFA Teflon (for NO_x) and PCTFE (for O_3) tubing. Temperature and relative humidity were measured by a Vaisala HMP60 Humidity and Temperature Probe. Ozone was measured with a dual beam ozone absorption monitor (2B Technologies Model 205) with a nominal accuracy and precision for 10s averages of 2% for concentrations above 50 ppbv. A Picarro Wavelength-Scanned Cavity Ring–Down Spectrometer (WS-CRDS) measures CH_4, CO_2, and water vapor (Picarro model 2301-f) with a specified 30s precision of <2 ppbv, <200 ppbv, and <150 ppmv, respectively. NO was measured by chemiluminescence (ECO PHYSICS Model CLD 88) with a stated precision of ~2%. A blue light LED photolytic converter (model 42i BLC2-395 manufactured by Air Quality Design, Inc.) was used to selectively convert NO_2 to NO for alternating measurements of NO_x (=NO+NO_2).

The instrument was cycled through the states of NO and total NO_x every 20 seconds. Calibrations were performed by O_3 titration with a NIST traceable NO standard (Scott-Marrin, Inc.) certified to within 5%. Full calibrations were performed before and after the entire flight series, with zero and span checks run routinely before and after each flight. Additionally, every 10 minutes the sample flow and the instrument's generated ozone was redirected through a pre-reaction chamber for a 40 second

5   period where the $NO+O_3$ reaction and subsequent chemiluminescence (CL) was allowed to take place before the detection cell, thereby tracking any matrix interferences that may add to the usual chemiluminescence in flight. These background signals interpolated between the 10 minute intervals were then subtracted from the continuous measurements. The interpolated NO_2 signal was noted to decay approximately exponentially after powering up, which sometimes affected the first 15-30 minutes of flight. The presumed artefact was successfully replicated in the lab with a constant NO_2 concentration, and was removed by

10   exponential detrending (see the Supplement). Winds are measured on the aircraft using a Duel-Hemisphere Global Positioning System combined with direct airspeed measurements, as described in Conley et al. (2014).

3.3 Flight Strategies

The flights specifically target that time of the day when the ABL is actively growing, but after passing the original rapid growth phase through the neutrally stable residual layer (RL). The main data set we use here comes from six flights sponsored by the

15   US EPA (labelled EPA in Figure 1) during the California Baseline Ozone Transport Study (CABOTS) that were conducted on the afternoons of 26-28 July and 4-6 August, 2016 from 1100 to 1500 PST spanning an approximate altitude range from near the surface up to ~3 km (Fig. S1). The aircraft flights consisted of 6–7 back and forth level and profiling legs of approximately 15 minutes duration (~60 km) up and back primarily along the mean wind direction (the valley axis) in order to capture the horizontal advection and vertical gradients of the measured scalars. The flight domain focused on the region of the SJV between

20   Fresno and Visalia with approximately two-thirds of the data collected below ~1 km, and missed approaches executed at each airport in order to sample to within a few meters of the ground. The flight days were selected in coordination with a team from NOAA's Earth System Research Laboratory operating a Tunable Optical Profiler for Aerosol and Ozone (TOPAZ) lidar in Visalia, California who have shown excellent agreement between the ozone data collected by the aircraft and lidar (Langford et al., 2019). Periodically the airplane would make deep vertical profiles from ~3 m to 3 km in addition to two or three other

25   profiling legs in order to diagnose the ABL top, its growth, and vertical profiles of the measured scalars.

Another fifteen flights were flown as part of a residual layer ozone study (from now on referred to as RLO flights) with a different flight pattern from the previous six (EPA) mentioned. The afternoon RLO flights were shorter in duration, did not cover the cross-valley dimension significantly, and consisted of direct transects from Fresno to Bakersfield and back with approximately six vertical profiles over approximately two and a half hours between 1230 and 1500 PST. Aside from take-

5   offs and landings at Fresno, these flights also included five very low passes at the Visalia, Delano, and Bakersfield airports (yellow circles in Fig. 1) in order to sample within ~5m of the surface. Despite their shorter duration and elongated domain, we include some analysis from these flights because they are more numerous and offer valuable complementary information to this study. Details of the RLO flights can be found in Caputi et al. (2019).

3.4 Scalar Budgeting Technique

10   The quantification and categorization of the essential processes that determine the surface concentrations of these pollutants can be executed by targeted flight campaigns. Such experiments provide a valuable service to the air quality community, especially modelers interested in testing their models on a process basis. After quantifying the individual terms of the budget equations, each term's relative importance can be weighted to provide a better understanding of the leading causes and factors affecting surface concentrations. Outlined in the seminal work of Lenschow et al. (1981) are original applications of the scalar

15   budgeting techniques used by Warner and Telford (1965) and Lenschow (1970) to help validate the newly developing technique of eddy covariance for measuring sensible heat fluxes by aircraft. Lenschow et al. (1981) went on to describe the effectiveness of well-designed aircraft ABL studies in determining the net source or sink (in their case for ozone) given the careful measurement of the other dynamically controlled terms. The technique can be generalized to any scalar budget (i.e. ozone, NO_x, water vapour, DMS, SO_2) to enable the calculation of important residuals including source or sink terms for non–

20   conserved species (Bandy et al., 2011; Conley et al., 2009; Faloona et al., 2009; Kawa and Pearson, 1989). Boundary layer heights were determined from each profile (approximately 8-12 per flight) based on the abrupt increase in potential temperature and drop in water vapor. The locations and time of each of these observations were then fit by a multilinear regression in time and the horizontal dimension to determine the ABL growth rates and gradients, which go into the budget to determine the entrainment velocity (Trousdell et al., 2016). Taking all the airborne data observed below the derived (linear) time-dependent

25   ABL depth we then perform the same multi-linear regression for all the scalars including potential temperature, water vapour,

O_3, NO_x, and CH_4. Aligning the x-axis with the mean wind direction, U, the advection and temporal trend terms of Equation 1 are derived from the coefficients of the linear regression fit to the ABL NO_x concentration field in horizontal direction and time (Conley et al., 2011). For a more in-depth discussion of the airborne budgeting technique and specifics for the budgets of methane and ozone in the SJV see Trousdell et al. (2016). The calculation of our emission estimates necessitates that we find an effective area of the ground that encompasses all the sources that have influenced the ABL air mass that is sampled. For each of the six flights we simply drew a polygon enclosing the latitude and longitude coordinates of the aircraft sampling within a time-dependent ABL whose height was parameterized using the linear regression mentioned above. The average area of this polygon was 5,200 km^2 (σ=940 km^2). To estimate an uncertainty in this area, we consider the average advection distance of the mean wind (~3 ms^{-1}) over the course of a large eddy turnover time (boundary layer height divided by convective velocity scale, which was ~ 7 minutes = 550 m/1.4 ms^{-1}) and multiply this on either end of the domain by an average cross-valley dimension (70 km) to generate a 'spread' in the sampled ABL area influenced by the surface flux field. Although this additional area represents less than 4% of the overall domain, we include a conservative 20% error in the error analysis for it. The total flight time in the SJV was twenty-two hours with eight hours in the ABL.

3.4.1 NO$_x$ Budget

Calculating the budget for NO_x requires evaluating the terms in the following equation:

$$\frac{\partial[NO_x]}{\partial t} = \frac{F_0}{z_i} + \frac{w_e \Delta[NO_x]}{z_i} - \frac{\overline{[NO_x]}}{\tau_{NOx}} - U\frac{\partial[NO_x]}{\partial x}, \tag{1}$$

The budget terms are (in order from left to right): a storage term ($\frac{\partial NO_x}{\partial t}$), the difference between the surface flux (F_0) and entrainment flux which is comprised of the entrainment velocity (w_e) and the jump in NO_x concentration ($\Delta[NO_x]$) across the entrainment zone divided by ABL height (z_i), the chemical loss term which is the mean NO_x concentration ($[NO_x]$) divided by the photochemical lifetime of NO_x (τ_{NOx}) and horizontal advection ($-U\frac{\partial NO_x}{\partial x}$). Unlike our other budgets, calculating the NO_x budget requires estimating the loss term because of its short photochemical lifetime. The oxidation rate of NO_x is principally controlled in the daytime by reaction with OH. Therefore, the rate constant k_{NO2+OH} was estimated from the equation and data presented for termolecular reactions given by JPL in their chemical kinetics publication 15-10 (Burkholder, 2015), with an average temperature and pressure taken from our flight data (average effective first order reaction rate, k_{NO2+OH}[M] ~

1.0x10^{-11} cm^3 molec^{-1} s^{-1}.) The median midday peak OH we chose to use in our calculation was observed in a different study to be approximately 6-8x10^6 molec cm^{-3} in the San Joaquin Valley (Brune et al., 2016), with a flight duration average of about 6 x10^6 molec cm^{-3}, which yields an average afternoon NO$_x$ photochemical lifetime, τ_{NO_x}, of ~4.6 (±0.08) hours for the six flights.

3.4.2 Error Analysis

The error for each derivative term in our multilinear regressions is a root mean square (RMS) error derived in the fit. The entrainment fluxes are comprised of the entrainment velocity and a scalar delta term. The delta term error was assigned to be -1.0 ppb for NO$_x$ and -50 ppb for methane based on variations in the data estimated by eye from inspection of the many vertical profiles. The entrainment velocity estimates are obtained from (see Supplement section S1): derivatives of ABL height, whose errors were previously mentioned, and a term from the WRF model (subsidence, or vertical velocity), which we have estimated as a conservative 0.5 cm s^{-1}, and the horizontal wind at ABL height assigned an error of 0.2 ms^{-1} based on the measurement capabilities of the instrument (Conley et al. 2014). The same error for horizontal winds near ABL height applies to the ABL horizontal winds used in calculating the advection terms. The NO$_x$ equation has in it a chemical loss term with an error from the uncertainty estimate equation for termolecular reactions given by JPL in their chemical kinetics publication 15-10, and the error in averaged ABL [NO$_2$], employed in the chemical loss term, was taken as one standard deviation of all the measurements. Estimated emission terms are residual terms within the respective budget equations. Their errors are calculated by adding the relative errors of all the other terms in the budget in quadrature. The regional area used to scale up the emission flux was assigned an error of 20 percent. The error in our average emission rates for NO$_x$ and CH$_4$ for all of the flights is a standard error of the mean (the standard deviation of the estimates divided by $\sqrt{6}$.) We believe that the errors in our emission estimate on a given flight day are likely much larger than any actual day-to-day variability, so the repeated flight dates amount to multiple measurements of a value that is approximately constant, therefore we consider it appropriate to treat the reported error of regional emissions as the standard deviation of the mean. In other words, while the emission estimate from a single flight on any given day is quite a noisy measurement, the repeated experiment can build confidence in the average result.

4 Results and Discussion

In the following section we present a variety of inferences gleaned from the three scalar budgets performed: for NO_x to derive regional surface emissions (4.1.1), for O_3 to derive afternoon photochemical production rates (4.1.2) and to see how that fits into the overall diurnal budget of ozone (4.1.2.1), and finally for CH_4 to derive regional emissions (4.1.3). Because of the large discrepancy between our estimates of NO_x emissions and that of the state inventory, we further explore possible reasons to explain the difference. The first is the hypothesis put forward by Almaraz et al. (2018) that there is a substantial source of NO from fertilized agricultural soils that is not accounted for in current state inventories (4.1.1.1). The second is the possibility that the Soberanes Fire in the mountains of the Coast Range approximately 200 km to the west (see Fig. 1) may have influenced our NO_x budget in the ABL around Fresno (4.1.1.2). The third explores the bias introduced by measuring only during the afternoon when NO_x emissions are thought to be highest (4.1.1.3), and the fourth discusses the possibility of a chemical interference in the measurement of NO_2, which in our system relies on photolysis followed by the chemiluminescence measurement of NO (4.1.1.4). The interference hypothesis is further explored by calculating Leighton ratios (4.1.1.5) in order to determine if the observed NO_2:NO ratios appear consistent with the theoretical photostationary state between O_3, NO, and NO_2 expressed in the Leighton ratios. This latter point leads naturally to the discussion of our estimates of ozone photochemical production (4.1.2) because it is, in principle, related to deviations in the observed Leighton ratios. Next, we present the observed spatial patterns of these scalars in the ABL calculating their horizontal autocorrelation lengths (4.2) to potentially infer emissions heterogeneity.

4.1 Budgets

In a future companion paper we will present the surface sensible heat fluxes for our flight region via two independent methods. The first being a turbulence analysis of the horizontal ABL winds using mixed-layer similarity considerations, the second a scalar budget analysis – in exactly the same manner as what is done for chemical species in this work – for potential temperature in the ABL, and finally comparing these to the output of the land surface parameterization of the WRF model. The results support each other and afford us added assurance in the budgeting technique. Supporting information from 15 additional flights in the SJV are presented for a project focused on studying ozone over the diurnal cycle, with a focus on residual layer ozone, and used for some of the analysis (hereupon referred to as 'RLO' flights). In general, we expect the EPA flights to yield better

results because they were longer in duration and more geographically focused targeting a complete midday budget of the scalars. Nevertheless, we performed the same analysis on the midday RLO flights and there do appear to be significant differences between the two domains (see Figure 1) when looking at the averaged quantities between the campaigns. For example, the entrainment rates for the entire region down to the southern end of the SJV at Bakersfield are nearly 50% larger than those around Fresno/Visalia. This is an interesting finding and one that is consistent with generally deeper boundary layers found in the southern end of the SJV as pointed out in previous studies (Bianco et al., 2011; Trousdell et al., 2016).

4.1.1 NO_x Emissions

NO_x ABL data were filtered by eliminating data greater than one standard deviation above the mean before being analysed in order to remove the skewness from the distributions induced by numerous spikes encountered in the late afternoons. Variations of this threshold from 1-3 standard deviations did not change the mean flight concentration by more than 2-3 percent so the exact threshold was not considered critical for our analysis. The data filtering was done to eliminate the spikes which were consistently encountered throughout the latter part of the flights, each lasting no more than a few minutes and uncorrelated with any other species measured (CO_2, CH_4, and O_3.) We conjecture that their source may have been something in the fire smoke entrained in the late afternoon ABL that caused a transient interference in the NO_2 photolytic chamber (they were not observed in the NO measurements.) Furthermore, as we discuss later in conjunction with Fig. 5, the influence of the fires on NO_x measured by the surface network (~1 ppbv) appears to be minimal during the six EPA flights relative to the clear signal enhancements in CO (~50 ppbv) and PM2.5 (~10 μgm^{-3}). Because the spikes were only encountered in the later afternoon their influence was particularly troublesome in estimates of the secular trend in NO_x. In four cases, simply removing the spikes from the ABL data set permitted a reasonable estimate of the afternoon trend, but on two flights we resorted to using data from the CARB monitoring network (https://www.arb.ca.gov/adam/hourly/hourly1.php). The trend established was the average of three station trends (from 11:00-16:00 PST) throughout the region: Fresno-Garland, Visalia-N. Church St., and Hanford-S. Irwin St. (the white diamond in Fig. 1 just west of Visalia). The estimates from the surface network and aircraft were very comparable for the other four flights where both were measured (averages of -0.38 vs. -0.34 ppb h^{-1}, respectively.)

Results from the NO_x budgeting are shown in Table 1. The average -0.36 ppb h^{-1} secular trend of NO_x is similar in magnitude to dilution induced by entrainment (-0.30 ppb h^{-1}), with chemical loss (-1.4 ppb h^{-1}) and surface emission (1.3 ppb h^{-1})

approximately balancing out. Advection on average is not significant but on any given day (for instance, 07/29) it can be large, which has been found to be the case elsewhere for other scalars and geophysical settings (Conley et al., 2009; Conley et al., 2011; Faloona et al., 2009). The relative role of entrainment changes from day to day as well, when compared to the average chemical loss it is about fifteen percent but on two of the flights (07/27 and 28) it is almost double that relative magnitude.

5   Measured emissions for the flight region were averaged and converted to metric tons per day giving an estimate of 216 metric tons per day (± 33, standard error, see error analysis section 3.4.2). The California Air Resources Board's (CARB) total NO_x inventory, representative of the summer based on CARB's CEPAM 2016 SIP - Standard Emission Tool (available at: https://www.arb.ca.gov/app/emsinv/fcemssumcat/fcemssumcat2016.php, 2018b) is 103.7 metric tons per day for the three surrounding counties: Tulare, Fresno, and Kings in SJV (Fig. 1). The combined size of these three counties is about six times

10   the flight region area. Thus, we would expect the airborne sampling domain to be a subset of the three-county region; however, since ~86% of the NO_x sources in the CARB inventory are mobile for these counties and our sampling occurred in the vicinity of each county's major population centre (Visalia, Fresno, and Hanford) and one of the SJV's main traffic arteries (CA state highway 99), it may be reasonable to expect the countywide NO_x emissions to be mostly sampled by the flights. Calculated NO_x chemical lifetimes averaged out to be 4.62 hours ($\sigma= 0.08$) for all flights, based on the rate constant data for nitrogen

15   dioxide's reaction with the hydroxyl radical to form nitric acid. We discuss several possible explanations for the discrepancy in our emission estimate and those of the CARB inventory in the following sections: soil NO_x emissions from fertilized agriculture in the region, wildfire effluent impacts on the airborne measurements, the bias due to the daytime sampling times, and possible chemical interferences to the measurement.

4.1.1.1 Soil NO_x Emissions from Agriculture

20   CARB currently considers mobile sources to make up 86.3% of the total NO_x emissions and that agriculture contributions are negligibly small. Nonetheless, agriculture represents the largest source of nitrogen to the state in the form of synthetic fertilizers (32%) and animal feed (12%) with about half of what is being applied to crops being lost to the environment (Tomich, 2016). Parrish et al. (2017) studied the temporal change in the ozone design values for California air basins over the past three decades and three heavily agricultural regions stood out: San Joaquin Valley, Salton Sea (containing the Imperial Valley), and North

25   Central Coast (containing the Salinas Valley.) Parrish et al. (2017) went on to fit the trends of the air basins to that of the South Coast Air Basin in their mathematical model in order to optimize their parameters but in doing so had to leave out the data in

the SJV before 2000. From 1980 to 2000 the trend essentially plateaus for the SJV, and since 2000 the trend is anomalously slow in the Salinas Valley and has an uncommonly high offset in the Salton Sea. The authors go on to suggest that these irregularities in the decadal O_3 trends may be explained by agricultural emissions, and/or by some unspecified temperature-dependent VOC with a possible connection to agricultural practices as proposed by Pusede and Cohen (2012).

5   While the average NO_x surface concentration decreased in the SJV by about 9.3% over the years 2005-2008, the Sacramento, San Francisco and South Coast regions saw a range of 22.6 to 30% decrease (Russell et al., 2010). In addition, the modelling estimates of Almaraz et al. (2018) show concentrated regions of high NO emissions in the SJV (Figure 3), Salton Sea air basin, and the Salinas Valley with the greatest magnitude NO_x emissions from soils for the state in these areas. In their model for soil NO_x, temperature was tracked as well as water filled pore space and nitrogen availability. Following a sensitivity analysis,

10   they found temperature to be one of the primary factors influencing soil NO_x emissions in the presence of excessive application of fertilizers where soil microbial communities increase the availability of nitrogen. We found a weak correlation (r^2=0.18) between our emission estimates and the ABL potential temperature, which should be just a little lower than the surface air temperature so we consider it as a decent proxy for soil temperature. Looking at the number of violations of the maximum 8-hour daily average O_3 (MDA8) standard for the counties of the SJV (data provided by CARB) over the past decade indicates

15   no observable trends outside of the two counties Kern and Tulare that contain some of the larger urban centres: Bakersfield, Visalia, and Hanford (Figure 4). While the SJV air basin as a whole may be showing slight decreases in MDA8 O_3 standard violations much of its rural areas are not. In a satellite study Russell et al. (2010) point out that changes to the spatial extent of NO_2 in the SJV are slower than other regions of the state. Other regions with stronger urban influences show significant shrinkage of the average NO_2 cloud around major urban centres while the SJV is largely an amorphous cloud of NO_2 in the

20   satellite images. Nevertheless, two other counties with major urban centres: Fresno County containing the city of Fresno, and San Joaquin County with Stockton do not show decreasing trends in the max 8-hour daily ozone yearly trend since 2006. Pusede and Cohen (2012) present satellite data from 2007 to 2010 which shows a significant NO_2 cloud around the Stockton area and to a lesser extent one around Fresno, although the SJV as a whole shows more broad scale homogeneity than other regions in California.

4.1.1.2 Potential Influence from Wildfires

It is important to note that throughout the course of the EPA flights the Soberanes fire was burning along the Big Sur coast of California. The fire started on July 22, 2016 and lasted until October of the same year. From the NASA MODIS satellite, clear images can be seen of the fire smoke being advected out and above the valley ABL on some days (see Fig. 1). We found greater variability towards the end of the flights in the ABL NO_x data, which could possibly be explained by the entrainment of fire smoke as the ABL reaches its maximum height. Amongst the myriad of chemical emissions from wildland forest fires is NO_x (Urbanski et al., 2009) and globally Jaegle et al. (2005) estimate that biomass burning contributes ~14% of surface [NO_x]. Singh et al. (2012) sampled numerous fire plumes throughout California during 2008 and found very little NO_x (<0.5 ppb) near the source of the fires but that the plumes could later acquire NO_x by mixing with other air masses containing higher NO_x levels. When the fire plumes they measured mixed with substantially polluted urban air, ozone formation rates were found to be at their highest all across California in comparison to purely urban or rural air. Elevated levels of reactive nitrogen oxides (NO_y) have been observed in smoke from biomass burning which contain reservoir species for NO_x like peroxyacetyl nitrate (PAN) that can later release NO_x relevant to O_3 formation (Dreessen et al., 2016).

Taking CARB data from their Fresno-Garland surface site which falls within our flight region we looked at CO, PM2.5 and NO_x for the six EPA flight days. While we found a strong positive correlation between CO and PM2.5 we found no correlation between CO and NO_x. In a longer time series representative of the Soberanes fire (07/22/16-10/12/16) a small, positive yet weak correlation between CO and NO_x can be seen (see Figure 5). Because the leading term of chemical loss is directly proportional to NO_2 concentration in the NO_x budget equation (Eq. 1), a sensitivity test was run to see how changes in the NO_2 concentration affect the emission estimates. A change in 1 ppb of NO_2 on average changes the emission by 35 metric tons per day. Nevertheless, even though there was likely some influence of the fire on the regional NO_x levels, the contribution most likely entered the ABL top through entrainment, which in principle is accounted for in the budgeting method by changes in the average jump across the ABL (ΔNO_x).

Diurnal CARB surface data from the SJV was compared to NO_x measurements from the RLO flight data below 100 m and at night we see fairly good agreement between the two. During our afternoon ABL flights, however, there appears to be a positive bias in the flight data (Figure 6). This may be because the airborne data below 100 m (AGL) altitude was only able to be

collected during the low approaches and take-off and landings at the airports: Bakersfield, Delano, Fresno and Visalia, all of which are located in close proximity to CA Highway 99.

4.1.1.3 Potential Bias because of the Measurement Period

Considering a typical diurnal cycle of NO_x emissions in a region with a large urban influence, particularly traffic, our emission rate during the period of measurement can be roughly estimated to be about a factor 1.4 greater than the average emission rate over the entire diurnal cycle. This is based on work by de Foy (2018) who estimated diurnal profiles of emissions based on a model which took into consideration the timing of mobile sources and meteorological impacts on their concentration measurements in the Chicago area (see their fig. 9 modelled data). Furthermore, Russell et al. (2010) reported a 27% decrease in NO_2 concentrations on weekends for Fresno and Bakersfield. Because five of our six flights were on weekdays and the last flight was a Saturday, our sampling may be slightly biased toward weekdays. Assuming an average decrease of NO_x emissions on weekends to 0.73 the weekday rate, our average daily emission rate would be a factor of 1.04 (=(5.73/6.46)x(7/6)) higher than inventories, which average over 5 weekdays and 2 weekend days each week. Taken together, the timing of the flights relative to the inventory's average summer emission rate could lead to a positive bias in our measurements of ~45% (=1.4x1.04).

4.1.1.4 Possible Chemical Interference in NO_x Measurements

The photolytic converter setup was developed specifically to avoid the problem of converting nitrogen containing species other than NO_2, which has been well established for standard CL NO_x monitors employing a heated molybdenum catalyst (Dunlea et al., 2007). Reed et al. (2016) studied interferences in the photolytic NO_2 instruments and found PAN to be the most significant due to thermal decomposition in the lamp chamber, reporting that in their instrumental set up ~5% of the PAN is dissociated. Although this is likely a very small contribution in our study, where average ABL temperatures were ~305 K, there is a very real possibility of some compounds that decompose to NO_2 (e.g., peroxynitrates, RO_2NO_2, or possibly even alkyl nitrates, $RONO_2$) being present in large quantities in the wildfire plumes (Alvarado et al., 2010; Akagi et al., 2011) that we encountered over the valley on some days. The short-lived spikes discussed earlier were removed from our analysis, and even when included they did not significantly affect the reported average NO_x concentrations. Consequently, these transient interferences should not impact our estimates of regional NO_x emission rates. However, the time-dependent interference that was removed (see the Supplement), could be the result of some wildfire effluent compound coating the inside of the photolysis

cell and contributing on the aggregate to the average NO_x measurements. Inspection of the collection of all NO_x interferences observed in the field and post-field calibrations and zero tests, which were removed in the final data analysis, show that the largest impacts were around 2 ppbv NO_x in magnitude. Using the sensitivity to emission estimates we calculated and discussed above, the very largest imaginable uncorrected interference in our NO_x measurements could give rise to an overestimate in our

5 emissions of ~70 tons per day, reducing our result by about 32%.

4.1.1.5 The Leighton Ratio

Here we use a modified Leighton ratio, Φ' to estimate the possible range of interference to our measured NO_2. The Leighton ratio, Φ, is unity when the NO_x and ozone chemistry is in photostationary state (PSS) and there is no net ozone photochemical production. The ratio deviates above unity when some other chemical process produces NO_2, i.e. reactions involving peroxy

10 radicals augment the primary pathway of NO oxidation by O_3. This is usually associated with areas where NO_x concentrations are not too high like heavily polluted urban centres where there are greater sinks for peroxy radicals and the loss pathway of [OH] with NO_2 is significant (Cantrell et al., 1993;Volz-Thomas et al., 2003). Deviations below unity indicate possible strong local NO emissions or rapid changes in J_{NO2} so that PSS has not been reached (Ma et al., 2017). Equation 5 from Griffin et al. (2007) defines a modified ratio, Φ', where it is assumed that peroxy radicals ($RO_x \equiv RO_2 + HO_2$) alone are responsible for

15 deviations seen in the Leighton ratio:

$$\Phi = \frac{j_{NO2}[NO_2]}{k_1[NO][O_3]}, \qquad \Phi' = \frac{j_{NO2}[NO_2]}{k_1[NO][O_3]+k_2[NO][RO_x]}, \qquad (2)$$

Forcing the modified ratio to be unity we can solve for NO_2: reaction rates come from JPL kinetics data, the photolysis rate is from the NCAR Quick-TUV calculator (available at: http://cprm.acom.ucar.edu/Models/TUV/Interactive_TUV/, 2018c), [O_3] is from our flight data and [RO_x] is taken from measurements made near Bakersfield presented by Brune et al. (2016), taken

20 as their [HO_2^*] which includes some amount of [RO_2] interference ([HO_2^*]= 15 pptv during our flight times). Between the NO_2 concentrations observed on the EPA flights and the calculated NO_2 there is a correlation of R^2=0.50 and a difference in mean NO_2 of about 0.7 ppbv (6.6 for EPA flights and 5.9 ppbv calculated). This can be considered a conservative estimate for possible NO_2 measurement interference because the choice for [RO_x] is on the lower end of a range of possible values. Griffith et al. (2016) reported maximum measured values of HO_2^* from about 3 to 40 pptv from Pasadena, California in the summer

25 of 2010 with a corresponding NO_2 range of about 6-14 ppbv (approximate values are taken from the time frame of our flights

for comparison). From before, the sensitivity of our emission estimate to changes in NO_2 is 35 tons per day for every 1 ppb change to NO_2 therefore possible chemical interference accounts for 24.5 tons per day or a systematic error of +%11. From our EPA flights, we found a range of Φ values from 1-3.3 with an average of 1.87. For measurement conditions similar to ours (predominately rural) the reported values for Φ are between 1 and 3 (Cantrell et al., 1993; Volz-Thomas et al., 2003; Mannschreck et al., 2004), therefore we feel that the NO_2 measurements reported herein are not likely to be subject to interferences much greater than ~10%.

4.1.2 Ozone Photochemical Production

The ABL averaged ozone was 74 ppb (σ=9.8 ppb) from our flight data which is close to the summertime surface network average for that region. Looking at the CARB sites from Fresno, Tulare, and Kings counties within and close to our flight region and averaging over the flight hours (12-16PST) for the summer months (JJA) the average ozone concentration was 70 ppb (σ=13 ppb). The averaged ozone photochemical production was 6.3 ppb h^{-1} ($\pm$ 3.3) compared to rates found for the southern SJV to be between 4.1 and 14.2 ppb h^{-1} in summer (Trousdell et al., 2016). Kleinman et al. (2002) modelled ozone production rates using observed data for five major U.S. metropolitan areas and found median values ranging from 3.5 to 11.3 ppb h^{-1}.

The ozone budget breakdown is shown in Table 2. The VOC chemistry in the SJV is dependent on temperature. At moderate temperatures ozone production is VOC-limited while at higher temperatures less so based on work by Pusede and Cohen (2012). They speculate that the temperature independent part of the organic reactivity in the southern SJV has been decreasing over the past years in response to emission regulations and is what led to the sharp decrease in ozone exceedances from the mid-90's until 2010 (Pusede et al., 2014). They further propose that NO_x regulations will be the most effective way to reduce ozone exceedances in the future and as NO_x levels decrease the temperature-dependent aspect of ozone chemistry will be diminished because at higher temperatures it becomes even more NO_x-limited. Trousdell et al. (2016) also argued that the ozone production in their study from 11 flights south of Bakersfield in 2013/2014 was NO_x-limited based on their estimates of the VOC:NO_x ratio derived from their airborne measurements of CH_4 as a VOC proxy, and the surface network observation of NO_x. Another study by Brune et al. (2016) suggests that ozone production continues to increase with NO beyond about 1ppb, in contrast to how the 'weekend effect' is believed to occur; however, high values of NO mostly occurred in the Brune

et al. (2016) study during the early morning before the time frame of the Pusede et al. (2014) study (10-14 PST). The 'weekend effect' is a phenomenon where ozone production goes up on weekends as NO_x emissions decrease due to less motor vehicle traffic on the roads, particularly heavy duty diesel trucks. Marr and Harley (2002), using an air quality model with a customized motor vehicle emissions inventory on four days in August 1990 reported a 30% reduction of NO_x emissions on the weekends

5   in Central California, but noted that the response of the ozone concentrations to the emissions reduction differed throughout the modelling domain with slight decreases in the area of the SJV included in the model (from Stockton south to Fresno.) Russell et al. (2010) stated a 27% decrease in NO_x emissions on weekends for Fresno and Bakersfield, the largest cities in the SJV, from satellite data taken from the summers of 2005-2008. When we included the 15 additional (RLO) flights we found photochemical production rates of 7.2 ($\pm$ 4.0) ppb h^{-1} on weekdays (total of 15 flights) and 7.8 (± 2.4) ppb h^{-1} on the weekends

10   (total of 6 flights), and a correlation with NO_x concentrations ($r^2 = 0.35$, Figure 7) suggesting that NO_x-limited conditions prevail. The average NO_x concentrations were 8.5 (± 2.0) ppb weekday and 9.0 ($\pm$ 2.1) ppb weekend. No significant 'weekend effect' was observed in this data set but one possible cause is that of the weekend flight days only two were Sundays where the most significant NO_x reductions are seen and Saturday acts more like a transition day (Russell et al., 2010).

15   Assuming that RO_x is responsible for positive deviations from PSS we can, in principle, relate our ozone photochemical production rates to expected RO_x levels. Assuming that net ozone photochemical production is solely due to RO_x and making the simplifying assumptions that the reaction rates with NO of RO_2 is approximately equal to that of HO_2 (Mihelcic et al., 2003) we can estimate the gross photochemical production rate of ozone to be:

$$P(O_3) = k_{NO+HO2} * [RO_x][NO], \tag{3}$$

20   The reaction rate is for the reaction of NO with HO_2 (Burkholder, 2015). A similar approach is found in Mihelcic et al. (2003), who used it for calculating what they saw as an upper limit for $P(O_3)$, as well as Ma et al. (2017). Therefore, applying our own calculated *net* production rates and subtracting an estimated photochemical loss of -1ppb h^{-1} (due to photolysis and OH production, and similar to the values Pusede et al. (2014) reported from their observations 0.7- 1.4 ppb h^{-1}) to get a gross production rate we expect the values for RO_x to be a lower limit. Our results indicate a range of values 2.4-19.4 pptv with an

25   average of 10.2 pptv. Brune et al. (2016) show afternoon values of about 8 pptv HO_2 and 15 pptv HO_2* (including some RO_2

interference) in the SJV which is consistent with our findings because the airborne data are representative of a wide regional average. Our measurements are distinct from those made at the Bakersfield supersite during CalNex which is at the heart of an urban plume.

Next looking at our modified Leighton ratios, ϕ_I, and using our measured concentrations with the JPL rate constants and solving for RO_x we find an average value of 154 pptv. Assuming that this value is off by a factor of 3 as found by Mannschreck et al. (2004) this suggests an approximate average range for RO_x during our measurement period of 9-50 pptv, and is consistent with several past studies (Cantrell et al., 1993; Hauglustaine et al., 1996; Volz-Thomas et al., 2003; Handisides et al., 2003)) that found deviations in the Leighton ratio cannot be explained solely by the reaction of RO_x with NO.

4.1.2.1 Full Diurnal Budget of Ozone

Data from the SJV (Trousdell et al., 2016) indicate that O_3 production generally increases as you progress southward, as expected because of the predominant wind direction in the valley and the gradual accumulation of ozone precursors as the air mass moves upvalley (Cox, 2013). Like our budget equations, the prognostic equations of a State Implementation Plan (SIP) model track the different rate/derivative terms which sum to the total time derivative of any scalar of interest like ozone. Thus, it is important to know how these change over time, so here we present a diurnal analysis for our flight dates (Figure 8). Ozone data is taken from eight CARB sites within our flight region, and our average photochemical production rate is extrapolated across the daytime hours by scaling the average observed value during the flight interval throughout the rest of the day based on the time series of $J(O^1D)$ from the NCAR Quick-TUV calculator. The areas under the curves represent the total $[O_3]$; therefore, it can be seen that the contributions from photochemistry and mixing down from the RL (fumigation) are approximately comparable. Very similar 50-50 split contributions from these two terms have been presented by past studies (Kleinman et al., 1994; Lin, 2008; Neu et al., 1994).

Now, we present an analysis of the average diurnal cycle of $d[O_3]/dt$ and $d[O_x]/dt$ ($O_x = NO_2 + O_3$, used because in the morning NO_2 quickly photolyzes to form O_3) (Figure 9) for the SSJV based on our RLO aircraft observations. Average trends are taken across each ~2 h flight as well as estimated in between flights totalling eight estimates each day. Data are binned into 3 altitude layers: the lower boundary layer 0-200 m – within the nocturnal boundary layer as discussed by Caputi et al. (2019), the upper boundary layer 200-600 m (mainly the RL when it is present and within the afternoon ABL), and the buffer layer 600-2000 m. Looking at the near surface data from the RLO flights and Figure 8 we see similarity: a peak (dominated by fumigation

from the RL) around 08:00-09:00 PST, a zero crossing around 15:00 PST, and a max loss at 19:00 PST. The exact timing of these events may differ by about an hour or so, and we observed such discrepancies even between diurnal profiles from different CARB sites in the SJV (data not shown). Looking at the difference between the Bakersfield and Fresno sites we see a smaller peak an hour later at Fresno and a smaller yet slightly earlier max loss time than at Bakersfield. To get a better sense

5 of the peak loss rate, we compare the same results from the $d[O_x]/dt$ (Figure 9), which shows that the near surface drop in O_3 right after sunset is not simply due to titration by rush hour NO emissions because a very comparable loss is observed in O_x which is conserved under titration. Given the absence of both photochemistry and entrainment at dusk, we conclude that that large loss of O_3 must be occurring due to dry deposition in a severely stunted mixed layer. A more extensive analysis is needed to understand the variations in diurnal profiles of ozone production and loss across the SJV, but we propose it can be an

10 instructive exercise to focus on the time derivatives as we have done here.

4.1.3 Methane Emissions

The methane emission average, after conversion to more commonly reported units, was 438 gigagrams per year (± 143, standard error) or 50 Mg h^{-1} (± 15.5) which is approximately one-half the size of an estimate by Cui et al. (2017) that used inverse modelling from flight data with a CALGEM (California Greenhouse Gas Emissions Measurement) prior and found

15 about 80 Mg h^{-1} (± 17) for a region they labelled D1 in which our flights took place. Their D1 region contained: Kern, Tulare, Madera, Fresno, and Kings counties totalling about 58 billion square meters. The area used for calculating our emission here is the same area used in the NO_x calculation. Our flight region was about one-tenth the size of the D1 region, but the highest emission rates found in the Cui et al. (2017) study came from the region between Hanover and Visalia, on which our flights focused. Figure 10 shows our flight tracks overlaying the CALGEM emission inventories across the SJV. See Table 3 for a

20 breakdown of methane budget terms. A region of the SJV approximately 3.5 billion square meters was probed in a previous campaign from June through September 2013 and in June 2014 focused on the southern end of the SJV, particularly Bakersfield, reporting a measurement of 170 gigagrams per year (±125) (Trousdell et al., 2016). Jeong et al. (2016), similar to Cui et al. (2017), based on their CALGEM prior model found that 86% of the methane in the SJV is from dairies. Our flight area included one of two extremely dense areas of dairy operations in the valley focused around the intersection of three

25 counties: Kings, Tulare and Fresno. Looking at the CALGEM inventory for our flight areas we found an average source

apportionment for dairies to be 88%. Trousdell et al. (2016) used CALGEM emission inventories scaled to the 2013 total CH_4 emission estimate for the state of California of 41.1 TgCO2eq provided by CARB and then compared that to in-situ data and found top-down airborne to bottom-up inventory ratios of 3.6 and 2.4 for the two regions studied (Fresno wintertime and Bakersfield summertime, respectively.) Our current study found an overestimate by a factor of 2.2 for the EPA flights. The

5   site in Trousdell et al. (2016) with a value of 3.6 is dominated by emissions from petroleum operations (54%) based on the CALGEM inventory and took place during the winter while the other value mentioned come from regions dominated by dairy operations during summer. Cui et al. (2017) reported a ratio between their model inversion and CALGEM of 1.8, comparable to the value reported here and taking place in a similar region and season. Because the airborne measurements of our study take place during six summer days, comparisons with annually averaged inventories should be done with caution as methane

10   emissions from the dominant sources (dairies) are likely to be seasonally temperature dependent. For example, a recent study of two dairies in the SJV (Arndt et al., 2018) reported facility-wide winter emissions to be only 40-50% of those during summer sampling. If this very local study were applied to the annual variations throughout the region, it could, in principle, bring our estimates as well as those of Cui et al. (2017) in much closer congruence to the CALGEM inventory. More routine flights and applications of the budgeting methods outlined in this work could help further elucidate the accuracy of methane inventories.

15   **4.2 Autocorrelation Length Scales**

Autocorrelation lengths, or integral length scales, represent the distance over which a variable maintains a significant level of correlation with itself, or the minimum distance for which the variable becomes statistically independent (Tortell, 2005). Qualitatively we think of this as the "patchiness" of the scalar field, for our purposes in the horizontal dimensions. Correlation coefficients were calculated as a function of distance by using a spatial autocorrelation technique called Moran's I:

20   $$CC = \frac{N}{W} \frac{\sum_i \sum_j w_{ij}(x_i - \bar{x})(x_j - \bar{x})}{\sum_i (x_i - \bar{x})^2},$$ (4)

where w_{ij} is a weight matrix which is either zero or one if the points of a pair (i,j) are a certain distance from each other, N is the number of pairs that fall into that distance category, W is the total number of pairs in the data set, and x represents the scalar. For our purposes, this means that all pairs of distinct scalar measurements in our domain are created and then binned into discrete bins based on distance between the two points that make up the pair. Then for each distance category a correlation

coefficient is calculated, and the bin width chosen was 1000 m. All data was selected to be within the time dependent ABL and corrected to a common time and height within the ABL to remove biasing from temporal and vertical trends before the autocorrelation was run. The length scale was selected as the first crossing of the 0.37 line ($=e^{-1}$). The results averaged over the flights are: potential temperature (18 km), water vapour (18 km), ozone (30 km), methane (27 km), and NO_x (28 km).

5   Figures 11 and 12 show the horizontal distributions of the chemical species and the Moran's I decorrelation pattern for the flight of July 27. Temperature and water represent ABL scalars dominated by surface fluxes, so in principle their correlation lengths are related to the scale of heterogeneity in their surface sources (irrigated or fallow fields, plots of differing albedos, urban heat islands, etc.) In the case of ozone, photochemical production dominates in the afternoon requiring the mixing together of NO_x and VOC emissions. The more spatially diffuse pattern of CH_4 and NO_x, comparable to that of ozone, may

10   imply a preponderance of broad areal sources rather than localized emissions from cities (5-15 km) and/or highway traffic. This result for NO_x calls to mind the findings from Russell et al. (2010) and Pusede and Cohen (2012) previously mentioned which show broad scale homogeneity for NO_x concentrations in the SJV unlike in other regions of California where urban hotspots appear more localized.

5   Conclusion

15   Using 6 days of flight data covering the period of ABL growth during the afternoon we have estimated emissions estimates for NO_x and CH_4, and photochemical production rates of ozone while employing a budget which exposes the key processes affecting their ABL concentrations. Of particular interest are the advection terms which are very difficult to obtain in ground-based studies, and entrainment which is often not treated explicitly in models as it is fundamentally a turbulent, sub-grid process. Our emissions estimate for NO_x suggest, like other previous studies, that agriculture in the SJV maybe a greater source

20   of NO_x than previously thought and may be contributing to the delayed decrease in O_3 surface concentrations compared to other air basins in California. After exploring possible explanations for NO_x emission estimates larger than expected including: a potential 45% due to the afternoon, mostly weekday timing of the flights, and possible chemical interference accounting for at the very most 2 ppb to our average NO_2 we propose 79 tons per day as the lowest conceivable estimate possible after combining all of our conservative error estimates. With that our result is still significant because our study region accounts for

only a fraction of the respective source region of the inventory estimate. Therefore, more work needs to be done to investigate soil NO_x in the SJV as it offers a potential avenue for further air quality remediation by more efficient fertilizer usage in the valley. Emissions estimates from CALGEM for methane are possibly under-predicted by about one-half the actual for the SJV, in close agreement to other studies, but seasonality remains an important understudied factor. Finally, we suggest that

5   calculations of autocorrelation lengths for NO_x, CH_4, water vapour, and ozone should be employed in future satellite and airborne studies in order to better understand the heterogeneity of sources in the ABL.

Author Contribution

Justin Trousdell participated in the conceptualization, formal analysis, visualization, and writing of the manuscript. Dani Caputi and Jeanelle Smoot participated in data collection, analysis, and visualizations for the work. Ian Faloona took part in

10   conceptualization, funding acquisition, resources, methodologies, oversight of the project, and a significant portion of the writing. Stephen Conley was responsible for flying the aircraft and collecting the in-situ data.

Competing Interests

The authors declare that they have no competing interests.

Acknowledgements

15   We would like to thank San Juaquin Air Pollution Control District (SJVAPCD), NASA, San Francisco Bay Area Air Quality Management District (SFBAAQMD), California Air Resources Board (CARB), and the US EPA. This work was done with the support of Contract 2016.129 with the Bay Area Air Quality Management District, which was itself supported by the US EPA. We thank Scott Bohning and Saffet Tanrikulu for their support in making that contract happen in time for its coincidence with the California Baseline Ozone Transport Study. The work also benefited from the coincident support of the California

20   Air Resources Board agreement #14-308. I. Faloona's effort was supported by the USDA National Institute of Food and Agriculture, [Hatch project CA-D-LAW-2229-H, "Improving Our Understanding of California's Background Air Quality and

Near-Surface Meteorology"]. We thank the two anonymous reviewers for their thorough and critical reviews of this manuscript which helped clarify the text significantly.

References

Worldview: Explore Your Dynamic Planet: https://worldview.earthdata.nasa.gov/, 2018a.

CEPAM: 2016 SIP - Standard Emission Tool: https://www.arb.ca.gov/app/emsinv/fcemssumcat/fcemssumcat2016.php, access: 16 July 2018b.

Quick TUV Calculator: http://cprm.acom.ucar.edu/Models/TUV/Interactive_TUV/, 2018c.

Almaraz, M., Bai, E., Wang, C., Trousdell, J., Conley, S., Faloona, I., and Houlton, B. Z.: Agriculture is a major source of NOx pollution in California, Science Advances, 4, 8, 10.1126/sciadv.aao3477, 2018.

Arndt, C., Leytem, A. B., Hristov, A. N., Zavala-Araiza, D., Cativiela, J. P., Conley, S., Daube, C., Faloona, I., and Herndon, S. C.: Short-term methane emissions from 2 dairy farms in California estimated by different measurement techniques and US Environmental Protection Agency inventory methodology: A case study, Journal of Dairy Science, 101, 11461-11479, https://doi.org/10.3168/jds.2017-13881, 2018.

Bandy, A., Faloona, I. C., Blomquist, B. W., Huebert, B. J., Clarke, A. D., Howell, S. G., Mauldin, R. L., Cantrell, C. A., Hudson, J. G., Heikes, B. G., Merrill, J. T., Wang, Y. H., O'Sullivan, D. W., Nadler, W., and Davis, D. D.: Pacific Atmospheric Sulfur Experiment (PASE): dynamics and chemistry of the south Pacific tropical trade wind regime, Journal of Atmospheric Chemistry, 68, 5-25, 10.1007/s10874-012-9215-8, 2011.

Bianco, L., Djalalova, I. V., King, C. W., and Wilczak, J. M.: Diurnal Evolution and Annual Variability of Boundary-Layer Height and Its Correlation to Other Meteorological Variables in California's Central Valley, Boundary-Layer Meteorology, 140, 491-511, 10.1007/s10546-011-9622-4, 2011.

Brune, W. H., Baier, B. C., Thomas, J., Ren, X., Cohen, R. C., Pusede, S. E., Browne, E. C., Goldstein, A. H., Gentner, D. R., Keutsch, F. N., Thornton, J. A., Harrold, S., Lopez-Hilfiker, F. D., and Wennberg, P. O.: Ozone production chemistry in the presence of urban plumes, Faraday Discussions, 189, 169-189, 10.1039/c5fd00204d, 2016.

Burkholder, J. B., S. P. Sander, J. Abbatt, J. R. Barker, R. E. Huie, C. E. Kolb, M. J. Kurylo, V. L. Orkin, D. M. Wilmouth, and P. H. Wine: Chemical Kinetics and Photochemical Data for Use in Atmospheric Studies, Evaluation No. 18, Jet Propulsion Laboratory, Pasadena, CA, 2015.

Caputi, D. J., Faloona, I., Trousdell, J., Smoot, J., Falk, N., and Conley, S.: Residual Layer Ozone, Mixing, and the Nocturnal Jet in California's San Joaquin Valley, Atmos. Chem. Phys., 19, 4721-4740, 2019.

Cantrell, C. A., Shetter, R. E., Calvert, J. G., Parrish, D. D., Fehsenfeld, F. C., Goldan, P. D., Kuster, W., Williams, E. J., Westberg, H. H., Allwine, G., and Martin, R.: PEROXY-RADICALS AS MEASURED IN ROSE AND ESTIMATED FROM PHOTOSTATIONARY STATE DEVIATIONS, Journal of Geophysical Research-Atmospheres, 98, 18355-18366, 10.1029/93jd01794, 1993.

Christopher Small, and Joel E. Cohen: Continental Physiography, Climate, and the Global Distribution of Human Population, Current Anthropology, 45, 269-277, 10.1086/382255, 2004.

Conley, S. A., Faloona, I., Miller, G. H., Lenschow, D. H., Blomquist, B., and Bandy, A.: Closing the dimethyl sulfide budget in the tropical marine boundary layer during the Pacific Atmospheric Sulfur Experiment, Atmospheric Chemistry and Physics, 9, 8745-8756, 10.5194/acp-9-8745-2009, 2009.

Conley, S. A., Faloona, I. C., Lenschow, D. H., Campos, T., Heizer, C., Weinheimer, A., Cantrell, C. A., Mauldin, R. L., Hornbrook, R. S., Pollack, I., and Bandy, A.: A complete dynamical ozone budget measured in the tropical marine boundary layer during PASE, Journal of Atmospheric Chemistry, 68, 55-70, 10.1007/s10874-011-9195-0, 2011.

Cox, P., Delao, A., and A. Kormaniczak: The California Almanac of Emissions and Air Quality, California Air Resources Board, 246, 2013.

Cui, Y. Y., Brioude, J., Angevine, W. M., Peischl, J., McKeen, S. A., Kim, S. W., Neuman, J. A., Henze, D. K., Bousserez, N., Fischer, M. L., Jeong, S., Michelsen, H. A., Bambha, R. P., Liu, Z., Santoni, G. W., Daube, B. C., Kort, E. A., Frost, G. J., Ryerson, T. B., Wofsy, S. C., and Trainer, M.: Top-down estimate of methane emissions in California using a mesoscale inverse modeling technique: The San Joaquin Valley, Journal of Geophysical Research-Atmospheres, 122, 3686-3699, 10.1002/2016jd026398, 2017.

de Foy, B.: City-level variations in NOx emissions derived from hourly monitoring data in Chicago, Atmospheric Environment, 176, 128-139, 10.1016/j.atmosenv.2017.12.028, 2018.

Dreessen, J., Sullivan, J., and Delgado, R.: Observations and impacts of transported Canadian wildfire smoke on ozone and aerosol air quality in the Maryland region on June 9–12, 2015, Journal of the Air & Waste Management Association, 66, 842-862, 10.1080/10962247.2016.1161674, 2016.

Dunlea, E. J., Herndon, S. C., Nelson, D. D., Volkamer, R. M., San Martini, F., Sheehy, P. M., Zahniser, M. S., Shorter, J. H., Wormhoudt, J. C., Lamb, B. K., Allwine, E. J., Gaffney, J. S., Marley, N. A., Grutter, M., Marquez, C., Blanco, S., Cardenas, B., Retama, A., Villegas, C. R. R., Kolb, C. E., Molina, L. T., and Molina, M. J.: Evaluation of nitrogen dioxide chemiluminescence monitors in a polluted urban environment, Atmospheric Chemistry and Physics, 7, 2691-2704, 10.5194/acp-7-2691-2007, 2007.

Ewing, S. A., Christensen, J. N., Brown, S. T., Vancuren, R. A., Cliff, S. S., and Depaolo, D. J.: Pb Isotopes as an Indicator of the Asian Contribution to Particulate Air Pollution in Urban California, Environmental Science & Technology, 44, 8911-8916, 10.1021/es101450t, 2010.

Faloona, I., Conley, S. A., Blomquist, B., Clarke, A. D., Kapustin, V., Howell, S., Lenschow, D. H., and Bandy, A. R.: Sulfur dioxide in the tropical marine boundary layer: dry deposition and heterogeneous oxidation observed during the Pacific Atmospheric Sulfur Experiment, Journal of Atmospheric Chemistry, 63, 13-32, 10.1007/s10874-010-9155-0, 2009.

Faloona, I.C., S. Chiao, A. Eiserloh, R.J. Alvarez II, G. Kirgis, A.O. Langford, C.J. Senff, D. Caputi, A. Hu, L. T. Iraci, E. L. Yates, J. E. Marrero, J.-M. Ryoo, S. Conley, S. Tanrikulu, J. Xu, and T. Kuwayama, The California Baseline Ozone Transport Study (CABOTS), Bulletin of American Meteorological Society, *submitted*.

Fast, J. D., Gustafson Jr, W. I., Berg, L. K., Shaw, W. J., Pekour, M., Shrivastava, M., Barnard, J. C., Ferrare, R. A., Hostetler, C. A., Hair, J. A., Erickson, M., Jobson, B. T., Flowers, B., Dubey, M. K., Springston, S., Pierce, R. B., Dolislager, L., Pederson, J., and Zaveri, R. A.: Transport and mixing patterns over Central California during the carbonaceous aerosol and radiative effects study (CARES), Atmos. Chem. Phys., 12, 1759-1783, 10.5194/acp-12-1759-2012, 2012.

Garratt, J. R.: THE INTERNAL BOUNDARY-LAYER - A REVIEW, Bound.-Layer Meteorol., 50, 171-203, 10.1007/bf00120524, 1990.

Grab, S.: Mountains of the World: A Global Priority, edited by B. Messerli and J. D. Ives. Parthenon Publishing, New York and Carnforth, 1997. ISBN 1 850 70781 2, £48·00 (hardback) 495 pp, Land Degradation & Development, 11, 197-198, doi:10.1002/(SICI)1099-145X(200003/04)11:2<197::AID-LDR390>3.0.CO;2-U, 2000.

Griffin, R. J., Beckman, P. J., Talbot, R. W., Sive, B. C., and Varner, R. K.: Deviations from ozone photostationary state during the International Consortium for Atmospheric Research on Transport and Transformation 2004 campaign: Use of measurements and photochemical modeling to assess potential causes, Journal of Geophysical Research: Atmospheres, 112, doi:10.1029/2006JD007604, 2007.

Griffith, S. M., Hansen, R. F., Dusanter, S., Michoud, V., Gilman, J. B., Kuster, W. C., Veres, P. R., Graus, M., Gouw, J. A., Roberts, J., Young, C., Washenfelder, R., Brown, S. S., Thalman, R., Waxman, E., Volkamer, R., Tsai, C., Stutz, J., Flynn, J. H., Grossberg, N., Lefer, B., Alvarez, S. L., Rappenglueck, B., Mielke, L. H., Osthoff, H. D., and Stevens, P. S.: Measurements of hydroxyl and hydroperoxy radicals during CalNex-LA: Model comparisons and radical budgets, Journal of Geophysical Research: Atmospheres, 121, 4211-4232, doi:10.1002/2015JD024358, 2016.

Henne, S., Furger, M., Nyeki, S., Steinbacher, M., Neininger, B., de Wekker, S. F. J., Dommen, J., Spichtinger, N., Stohl, A., and Prevot, A. S. H.: Quantification of topographic venting of boundary layer air to the free troposphere, Atmospheric Chemistry and Physics, 4, 497-509, 10.5194/acp-4-497-2004, 2004.

Huang, M., Carmichael, G. R., Adhikary, B., Spak, S. N., Kulkarni, S., Cheng, Y. F., Wei, C., Tang, Y., Parrish, D. D., Oltmans, S. J., D'Allura, A., Kaduwela, A., Cai, C., Weinheimer, A. J., Wong, M., Pierce, R. B., Al-Saadi, J. A., Streets, D. G., and Zhang, Q.: Impacts of transported background ozone on California air quality during the ARCTAS-CARB period - a multi-scale modeling study, Atmospheric Chemistry and Physics, 10, 6947-6968, 10.5194/acp-10-6947-2010, 2010.

Iacobellis, S. F., Commission., C. E., Agency., C. E. P., and Center., C. C. C.: Climate variability and California low-level temperature inversions : final paper, California Energy Commission, Sacramento, Calif., xii, 48 p. pp., 2009.

Jaegle, L., Steinberger, L., Martin, R. V., and Chance, K.: Global partitioning of NOx sources using satellite observations: Relative roles of fossil fuel combustion, biomass burning and soil emissions, Faraday Discussions, 130, 407-423, 10.1039/b502128f, 2005.

Jeong, S. G., Newman, S., Zhang, J. S., Andrews, A. E., Bianco, L., Bagley, J., Cui, X. G., Graven, H., Kim, J., Salameh, P., LaFranchi, B. W., Priest, C., Campos-Pineda, M., Novakovskaia, E., Sloop, C. D., Michelsen, H. A., Bambha, R. P., Weiss, R. F., Keeling, R., and Fischer, M. L.: Estimating methane emissions in California's urban and rural regions using multitower observations, Journal of Geophysical Research-Atmospheres, 121, 13031-13049, 10.1002/2016jd025404, 2016.

Jin, L., Harley, R. A., and Brown, N. J.: Ozone pollution regimes modeled for a summer season in California's San Joaquin Valley: A cluster analysis, Atmospheric Environment, 45, 4707-4718, 10.1016/j.atmosenv.2011.04.064, 2011.

Kawa, S. R., and Pearson, R.: AN OBSERVATIONAL STUDY OF STRATOCUMULUS ENTRAINMENT AND THERMODYNAMICS, Journal of the Atmospheric Sciences, 46, 2649-2661, 10.1175/1520-0469(1989)046<2649:aosose>2.0.co;2, 1989.

Kleinman, L., Lee, Y. N., Springston, S. R., Nunnermacker, L., Zhou, X. L., Brown, R., Hallock, K., Klotz, P., Leahy, D., Lee, J. H., and Newman, L.: OZONE FORMATION AT A RURAL SITE IN THE SOUTHEASTERN UNITED-STATES, Journal of Geophysical Research-Atmospheres, 99, 3469-3482, 10.1029/93jd02991, 1994.

Kleinman, L. I., Daum, P. H., Imre, D., Lee, Y. N., Nunnermacker, L. J., Springston, S. R., Weinstein-Lloyd, J., and Rudolph, J.: Ozone production rate and hydrocarbon reactivity in 5 urban areas: A cause of high ozone concentration in Houston, Geophysical Research Letters, 29, 10.1029/2001gl014569, 2002.

Lagarias, J. S., and Sylte, W. W.: DESIGNING AND MANAGING THE SAN JOAQUIN VALLEY AIR-QUALITY STUDY, Journal of the Air & Waste Management Association, 41, 1176-1179, 10.1080/10473289.1991.10466912, 1991.

Langford, A. O., Alvarez Ii, R. J., Kirgis, G., Senff, C. J., Caputi, D., Conley, S. A., Faloona, I. C., Iraci, L. T., Marrero, J. E., McNamara, M. E., Ryoo, J. M., and Yates, E. L.: Intercomparison of lidar, aircraft, and surface ozone measurements in the San Joaquin Valley during the California Baseline Ozone Transport Study (CABOTS), Atmos. Meas. Tech., 12, 1889-1904, 10.5194/amt-12-1889-2019, 2019.

Lenschow, D. H.: Airplane Measurements of Planetary Boundary Layer Structure, Journal of Applied Meteorology, 9, 874-884, 10.1175/1520-0450(1970)009<0874:amopbl>2.0.co;2, 1970.

Lenschow, D. H., Pearson, R., and Stankov, B. B.: ESTIMATING THE OZONE BUDGET IN THE BOUNDARY-LAYER BY USE OF AIRCRAFT MEASUREMENTS OF OZONE EDDY FLUX AND MEAN CONCENTRATION, Journal of Geophysical Research-Oceans, 86, 7291-7297, 10.1029/JC086iC08p07291, 1981.

Leukauf, D., Gohm, A., and Rotach, M. W.: Quantifying horizontal and vertical tracer mass fluxes in an idealized valley during daytime, Atmospheric Chemistry and Physics, 16, 13049-13066, 10.5194/acp-16-13049-2016, 2016.

Lin, C.-H.: Impact of Downward-Mixing Ozone on Surface Ozone Accumulation in Southern Taiwan, Journal of the Air & Waste Management Association, 58, 562-579, 10.3155/1047-3289.58.4.562, 2008.

Lin, M. Y., Fiore, A. M., Horowitz, L. W., Cooper, O. R., Naik, V., Holloway, J., Johnson, B. J., Middlebrook, A. M., Oltmans, S. J., Pollack, I. B., Ryerson, T. B., Warner, J. X., Wiedinmyer, C., Wilson, J., and Wyman, B.: Transport of Asian ozone pollution into surface air over the western United States in spring, Journal of Geophysical Research-Atmospheres, 117, 20, 10.1029/2011jd016961, 2012.

Ma, Y. F., Lu, K. D., Chou, C. C. K., Li, X. Q., and Zhang, Y. H.: Strong deviations from the NO-NO2-O-3 photostationary state in the Pearl River Delta: Indications of active peroxy radical and chlorine radical chemistry, Atmospheric Environment, 163, 22-34, 10.1016/j.atmosenv.2017.05.012, 2017.

Mannschreck, K., Gilge, S., Plass-Duelmer, C., Fricke, W., and Berresheim, H.: Assessment of the applicability of NO-NO2-O-3 photostationary state to long-term measurements at the Hohenpeissenberg GAW Station, Germany, Atmospheric Chemistry and Physics, 4, 1265-1277, 10.5194/acp-4-1265-2004, 2004.

Marr, L. C., and Harley, R. A.: Modeling the effect of weekday-weekend differences in motor vehicle emissions on photochemical air pollution in central California, Environmental Science & Technology, 36, 4099-4106, 10.1021/es020629x, 2002.

Maurizi, A., Russo, F., and Tampieri, F.: Local vs. external contribution to the budget of pollutants in the Po Valley (Italy) hot spot, Sci. Total Environ., 458, 459-465, 10.1016/j.scitotenv.2013.04.026, 2013.

Mihelcic, D., Holland, F., Hofzumahaus, A., Hoppe, L., Konrad, S., Musgen, P., Patz, H. W., Schafer, H. J., Schmitz, T., Volz-Thomas, A., Bachmann, K., Schlomski, S., Platt, U., Geyer, A., Alicke, B., and Moortgat, G. K.: Peroxy radicals during BERLIOZ at Pabstthum: Measurements, radical budgets and ozone production, Journal of Geophysical Research-Atmospheres, 108, 17, 10.1029/2001jd001014, 2003.

Miller, S. T. K., Keim, B. D., Talbot, R. W., and Mao, H.: Sea breeze: Structure, forecasting, and impacts, Rev. Geophys., 41, 31, 10.1029/2003rg000124, 2003.

Neu, U., Kunzle, T., and Wanner, H.: ON THE RELATION BETWEEN OZONE STORAGE IN THE RESIDUAL LAYER AND DAILY VARIATION IN NEAR-SURFACE OZONE CONCENTRATION - A CASE-STUDY, Boundary-Layer Meteorology, 69, 221-247, 10.1007/bf00708857, 1994.

Noppel, H., and Fiedler, F.: Mesoscale heat transport over complex terrain by slope winds - A conceptual model and numerical simulations, Bound.-Layer Meteorol., 104, 73-97, 10.1023/a:1015556228119, 2002.

Parrish, D. D., Aikin, K. C., Oltmans, S. J., Johnson, B. J., Ives, M., and Sweeny, C.: Impact of transported background ozone inflow on summertime air quality in a California ozone exceedance area, Atmospheric Chemistry and Physics, 10, 10093-10109, 10.5194/acp-10-10093-2010, 2010.

Parrish, D. D., Young, L. M., Newman, M. H., Aikin, K. C., and Ryerson, T. B.: Ozone Design Values in Southern California's Air Basins: Temporal Evolution and US Background Contribution, Journal of Geophysical Research-Atmospheres, 122, 11166-11182, 10.1002/2016jd026329, 2017.

Pfister, G. G., Parrish, D. D., Worden, H., Emmons, L. K., Edwards, D. P., Wiedinmyer, C., Diskin, G. S., Huey, G., Oltmans, S. J., Thouret, V., Weinheimer, A., and Wisthaler, A.: Characterizing summertime chemical boundary conditions for airmasses entering the US West Coast, Atmospheric Chemistry and Physics, 11, 1769-1790, 10.5194/acp-11-1769-2011, 2011.

Pusede, S. E., and Cohen, R. C.: On the observed response of ozone to NOx and VOC reactivity reductions in San Joaquin Valley California 1995-present, Atmospheric Chemistry and Physics, 12, 8323-8339, 10.5194/acp-12-8323-2012, 2012.

Pusede, S. E., Gentner, D. R., Wooldridge, P. J., Browne, E. C., Rollins, A. W., Min, K. E., Russell, A. R., Thomas, J., Zhang, L., Brune, W. H., Henry, S. B., DiGangi, J. P., Keutsch, F. N., Harrold, S. A., Thornton, J. A., Beaver, M. R., St Clair, J. M., Wennberg, P. O., Sanders, J., Ren, X., VandenBoer, T. C., Markovic, M. Z., Guha, A., Weber, R., Goldstein, A. H., and Cohen, R. C.: On the temperature dependence of organic reactivity, nitrogen oxides, ozone production, and the impact of emission controls in San Joaquin Valley, California, Atmospheric Chemistry and Physics, 14, 3373-3395, 10.5194/acp-14-3373-2014, 2014.

Reed, C., Evans, M. J., Di Carlo, P., Lee, J. D., and Carpenter, L. J.: Interferences in photolytic NO2 measurements: explanation for an apparent missing oxidant?, Atmospheric Chemistry and Physics, 16, 4707-4724, 10.5194/acp-16-4707-2016, 2016.

Rotach, M. W., Wohlfahrt, G., Hansel, A., Reif, M., Wagner, J., and Gohm, A.: THE WORLD IS NOT FLAT Implications for the Global Carbon Balance, Bulletin of the American Meteorological Society, 95, 1021-+, 10.1175/bams-d-13-00109.1, 2014.

Rotach, M. W., Gohm, A., Lang, M. N., Leukauf, D., Stiperski, I., and Wagner, J. S.: On the Vertical Exchange of Heat, Mass, and Momentum Over Complex, Mountainous Terrain, Front. Earth Sci., 3, 14, 10.3339/feart.2075.00076, 2015.

Russell, A. R., Valin, L. C., Bucsela, E. J., Wenig, M. O., and Cohen, R. C.: Space-based Constraints on Spatial and Temporal Patterns of NOx Emissions in California, 2005-2008, Environmental Science & Technology, 44, 3608-3615, 10.1021/es903451j, 2010.

Ryerson, T. B., Andrews, A. E., Angevine, W. M., Bates, T. S., Brock, C. A., Cairns, B., Cohen, R. C., Cooper, O. R., de Gouw, J. A., Fehsenfeld, F. C., Ferrare, R. A., Fischer, M. L., Flagan, R. C., Goldstein, A. H., Hair, J. W., Hardesty, R.

M., Hostetler, C. A., Jimenez, J. L., Langford, A. O., McCauley, E., McKeen, S. A., Molina, L. T., Nenes, A., Oltmans, S. J., Parrish, D. D., Pederson, J. R., Pierce, R. B., Prather, K., Quinn, P. K., Seinfeld, J. H., Senff, C. J., Sorooshian, A., Stutz, J., Surratt, J. D., Trainer, M., Volkamer, R., Williams, E. J., and Wofsy, S. C.: The 2010 California Research at the Nexus of Air Quality and Climate Change (CalNex) field study, Journal of Geophysical Research-Atmospheres, 118, 5830-5866, 10.1002/jgrd.50331, 2013.

Singh, H. B., Cai, C., Kaduwela, A., Weinheimer, A., and Wisthaler, A.: Interactions of fire emissions and urban pollution over California: Ozone formation and air quality simulations, Atmospheric Environment, 56, 45-51, 10.1016/j.atmosenv.2012.03.046, 2012.

Stull, R. B.: An Introduction to Boundary Layer Meteorology, Kluwer Academic Publishers, 1988.

Tomich, T. P.: The California nitrogen assessment : challenges and solutions for people, agriculture, and the environment, University of California Press, Oakland, California, xxviii, 304 pagesv pages pp., 2016.

Tortell, P. D.: Small-scale heterogeneity of dissolved gas concentrations in marine continental shelf waters, Geochemistry Geophysics Geosystems, 6, 16, 10.1029/2005gc000953, 2005.

Trousdell, J. F., Conley, S. A., Post, A., and Faloona, I. C.: Observing entrainment mixing, photochemical ozone production, and regional methane emissions by aircraft using a simple mixed-layer framework, Atmospheric Chemistry and Physics, 16, 15433-15450, 10.5194/acp-16-15433-2016, 2016.

Urbanski, S. P., Hao, W. M., and Baker, S.: Chemical Composition of Wildland Fire Emissions, in: Wildland Fires and Air Pollution, edited by: Bytnerowicz, A., Arbaugh, M. J., Riebau, A. R., and Andersen, C., Developments in Environmental Science, Elsevier Science Bv, Amsterdam, 79-107, 2009.

Volz-Thomas, A., Patz, H. W., Houben, N., Konrad, S., Mihelcic, D., Klupfel, T., and Perner, D.: Inorganic trace gases and peroxy radicals during BERLIOZ at Pabstthum: An investigation of the photostationary state of NOx and O-3, Journal of Geophysical Research-Atmospheres, 108, 15, 10.1029/2001jd001255, 2003.

Warner, J., and Telford, J. W.: A CHECK OF AIRCRAFT MEASUREMENTS OF VERTICAL HEAT FLUX, Journal of the Atmospheric Sciences, 22, 463-&, 10.1175/1520-0469(1965)022<0463:acoamo>2.0.co;2, 1965.

Watson, J. G., Chow, J. C., Bowen, J. L., Lowenthal, D. H., Hering, S., Ouchida, P., and Oslund, W.: Air quality measurements from the Fresno Supersite, Journal of the Air & Waste Management Association, 50, 1321-1334, 10.1080/10473289.2000.10464184, 2000.

Wheeler, N. J. M., Craig, K. J., and Reid, S. B.: An Investigation of Aloft Model Performance for Two Episodes During the 2000 Central California Ozone Study, in: Air Pollution Modeling and Its Application Xx, edited by: Steyn, D. G., and Rao, S. T., NATO Science for Peace and Security Series B-Physics and Biophysics, Springer, Dordrecht, 603-607, 2010.

Flight Date	$\partial[NO_x]/\partial t$ Storage (ppbv h^{-1})	1 σ	$-U(\partial[NO_x]/\partial x)$ Advection (ppbv h^{-1})	1 σ	$w_e\,\Delta[NO_x]/z_i$ Entrainment (ppbv h^{-1})	1 σ	$-k[OH][NO_2]$ Chem Loss (ppbv h^{-1})	1 σ	F_0/z_i Emission (ppbv h^{-1})	1 σ	τ_{NO2} lifetime (h)	1 σ	Avg. ABL [NO$_x$] (ppbv)	1 σ	Avg. ABL [NO] (ppbv)	1 σ	Regional Emissions (tonnes d^{-1})	1 σ
7/27/16	-0.29	0.04	0.01	0.03	-0.52	0.37	-1.5	1.1	1.7	1.1	4.68	1.46	9.0	3.5	1.9	3.6	274	187
7/28/16	-0.09	0.07	-0.09	0.03	-0.52	0.39	-1.4	0.9	1.9	1.0	4.68	1.45	8.5	2.6	2.1	3.0	301	166
7/29/16	-0.44	0.07	0.30	0.05	-0.17	0.14	-1.8	2.1	1.2	2.1	4.69	1.47	9.6	8.8	1.4	7.9	182	324
8/4/16	-0.73	0.01	0.04	0.01	-0.30	0.21	-1.1	0.7	0.6	0.7	4.60	1.40	5.5	1.6	0.5	1.2	115	132
8/5/16	-0.83	0.03	-0.01	0.01	-0.15	0.13	-1.5	1.0	0.9	1.0	4.51	1.36	7.8	2.9	0.8	2.3	137	160
8/6/16	0.22	0.06	-0.02	0.01	-0.14	0.13	-1.3	0.8	1.7	0.9	4.55	1.37	7.8	2.4	1.8	3.8	286	155
Average	-0.36	0.05	0.04	0.02	-0.30	0.23	-1.4	1.1	1.3	1.1	4.62	1.42	8.0	3.6	1.4	3.7	216	187
Std. Dev.	0.4	0.02	0.1	0.01	0.2	0.1	0.2	0.5	0.5	0.5	0.08	0.05	1.4	2.6	0.6	2.3	81	69

Table 1 NO$_x$ budgets for the six EPA flights. All averages are calculated using ABL data only. The columns labeled '1σ' represent the estimated error in the preceding term with the same units.

Flight Date	$\partial[O_3]/\partial t$ Storage (ppbv h^{-1})	1 σ	$-U(\partial[O_3]/\partial x)$ Advection (ppbv h^{-1})	1 σ	$-v_d[O_3]$ Dry Deposition (ppbv h^{-1})	1 σ	$w_e \Delta[O_3]/z_i$ Entrainment (ppbv h^{-1})	1 σ	$\Delta[O_3]$ Jump (ppbv)	Avg. ABL [O$_3$] (ppbv)	$P_{net}(O_3)$ Photo.Prod. (ppbv h^{-1})	1 σ
7/27/16	1.24	0.12	-0.84	0.18	-2.98	1.59	-1.74	0.58	-5.0	89.6	6.80	1.71
7/28/16	6.06	0.19	-2.35	0.13	-2.47	1.32	1.04	0.48	3.0	70.2	9.83	1.43
7/29/16	-0.79	0.13	0.18	0.10	-2.81	1.52	-0.55	0.33	-5.0	76.9	2.40	1.56
8/4/16	0.95	0.05	-0.48	0.09	-2.11	1.11	-0.99	0.32	-5.0	75.7	4.53	1.16
8/5/16	6.45	0.05	-1.61	0.09	-2.11	1.13	-0.51	0.28	-5.0	59.9	10.69	1.17
8/6/16	3.00	0.05	0.04	0.05	-2.33	1.24	-0.47	0.29	-5.0	70.9	5.77	1.28
Average	2.8	0.1	-1.0	0.1	-2.5	1.3	-0.5	0.4	-3.4	74.5	6.9	1.4
Std. Dev.	3.3		1.0		0.4		1.0		3.6	10.8	3.5	

Table 2 O$_3$ budgets for the six EPA flights. All averages are calculated using ABL data only. The columns labeled 1σ represent the estimated error in the preceding term with the same units.

Flight Date	$\partial[CH_4]/\partial t$ Storage (ppbv h^{-1})	1 σ	$-U(\partial[CH_4]/\partial x)$ Advection (ppbv h^{-1})	1 σ	$w_e\, \Delta[CH_4]/z_i$ Entrainment (ppbv h^{-1})	1 σ	Emission Rate (Gg yr^{-1})	1 σ	$\Delta[CH_4]$ Jump (ppbv)	Avg. ABL [CH$_4$] (ppbv)
7/27/16	-40.5	1.89	-3.4	2.20	-69.4	22.1	487	362	-200	2170
7/28/16	-8.0	0.91	-6.9	0.70	-69.5	24.6	982	447	-200	2027
7/29/16	-10.5	1.32	9.3	0.92	-22.1	12.8	31	177	-200	2021
8/4/16	-5.7	0.58	-3.4	0.21	-39.7	12.7	686	290	-200	2022
8/5/16	-5.3	0.45	0.0	0.24	-20.5	10.8	223	170	-200	1993
8/6/16	-3.1	0.49	1.6	0.26	-18.9	11.6	220	190	-200	1996
Average	-12.2	0.9	-0.5	0.8	-40.0	15.8	438	273	-200	2038
Std. Dev.	14.1		5.6		24.0		352			66
Std. Error							144			

Table 3 CH$_4$ budgets for the six EPA flights. The columns labeled 1σ represent the estimated error in the preceding term with the same units.

Figure 1. Satellite view of the San Joaquin Valley. Yellow circles are key sites which are labelled. The green lines are the combined tracks from the EPA flights and the blue are from the RLO flights. White diamonds are CARB surface stations. Active fires on the ground can be seen as small red outlines to the Northwest of the Chews Ridge site (available at: https://worldview.earthdata.nasa.gov/, 2018a) from July 27, 2016. Major mountain ranges are labelled in white. The three shaded regions are Fresno County in blue, bottom left in red is Kings County, and bottom right in white is Tulare County.
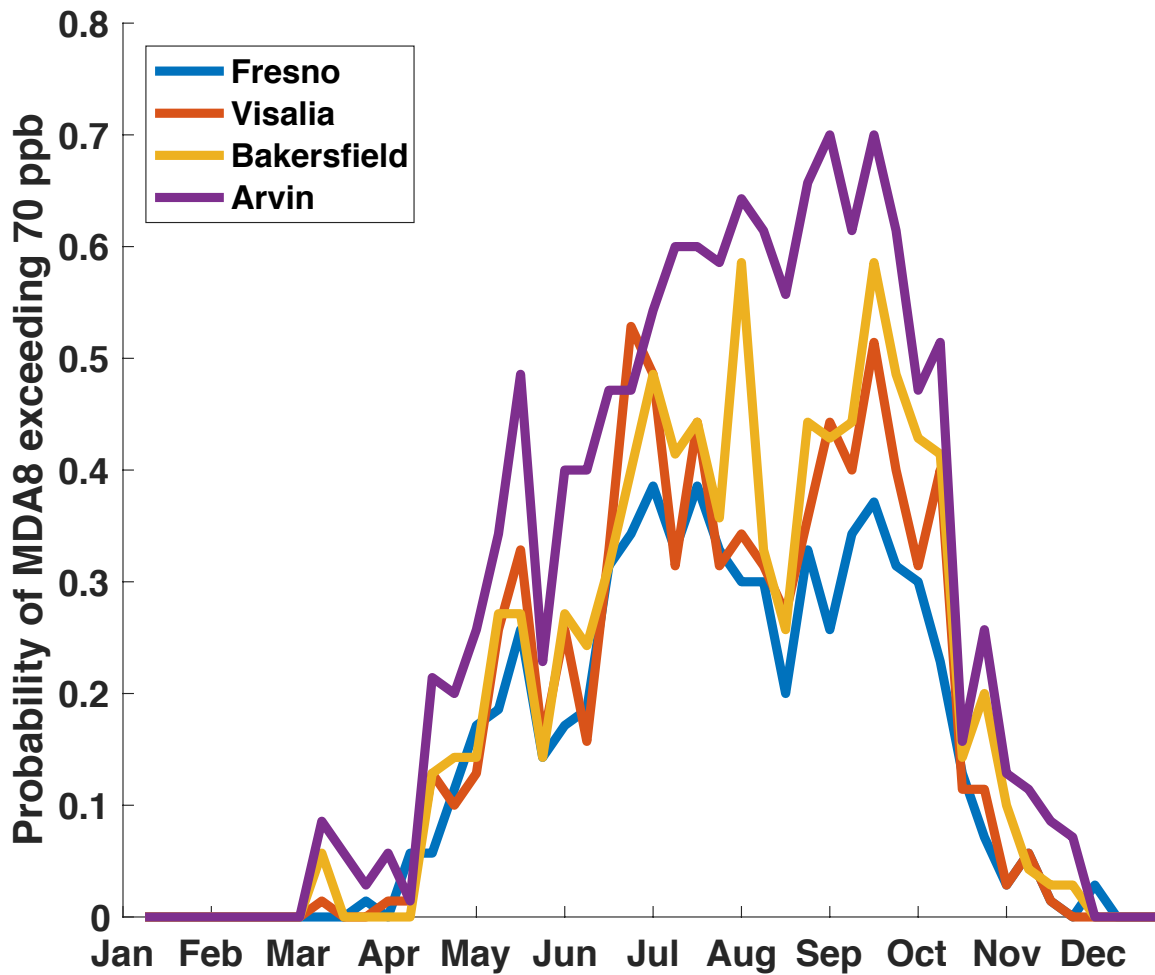
Figure 2. The probability of an MDA8 exceeding 70 ppb each week of an annual cycle at four sites in the SJV, from north to south: Fresno, Visalia, Bakersfield, and Arvin (see Fig. 1). The data are from the CARB network from 2006 – 2015.
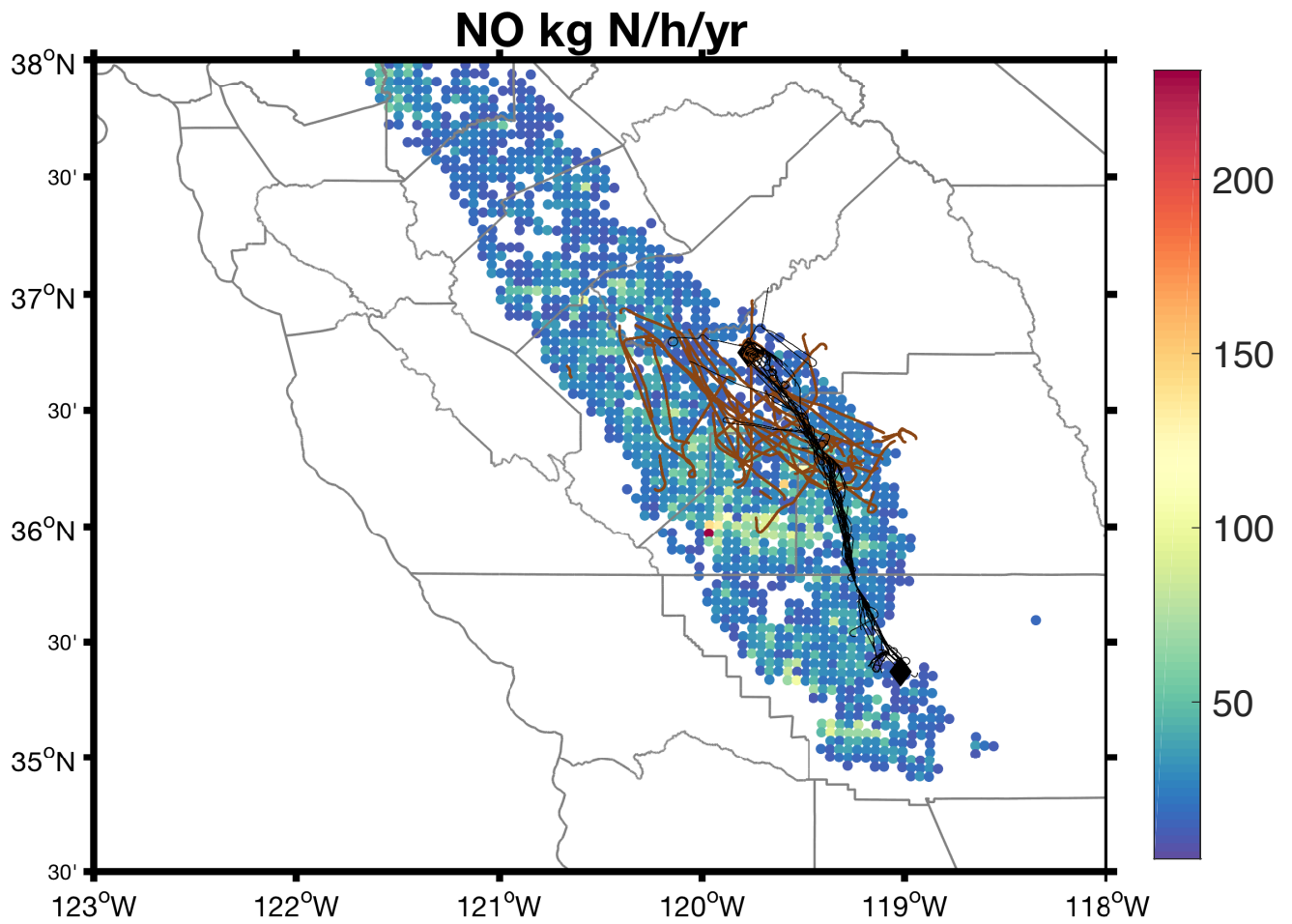
Figure 3. Soil NO emissions in kg N per hectare per year for the SJV with flight tracks (data from Almaraz et al. (2018)). Significant sources for soil NO show up in the middle SJV in Kings County.
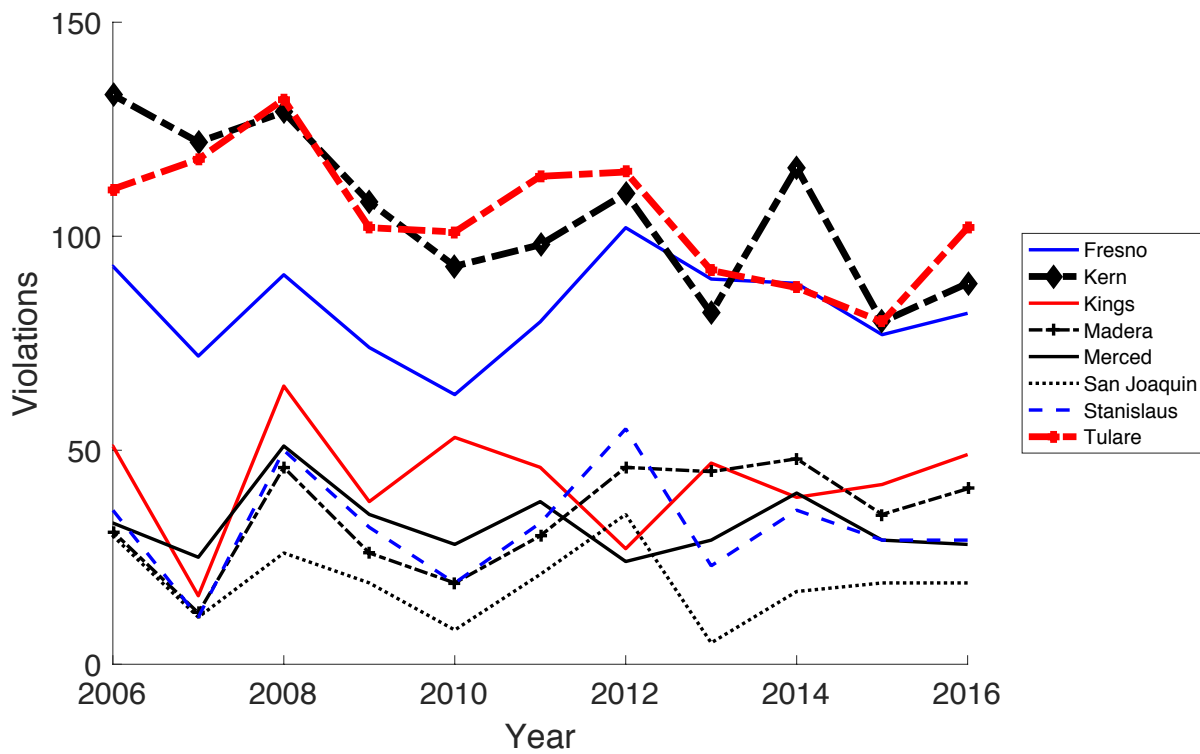
Figure 4. Tulare and Kern counties show signs of a downward trend for ozone violations, while the other counties of the SJV, which are largely rural, don't show a clear downward trend. Los Angeles County is shown as a reference for comparison with the South Coast Basin. Data provided by California Air Resources Board.
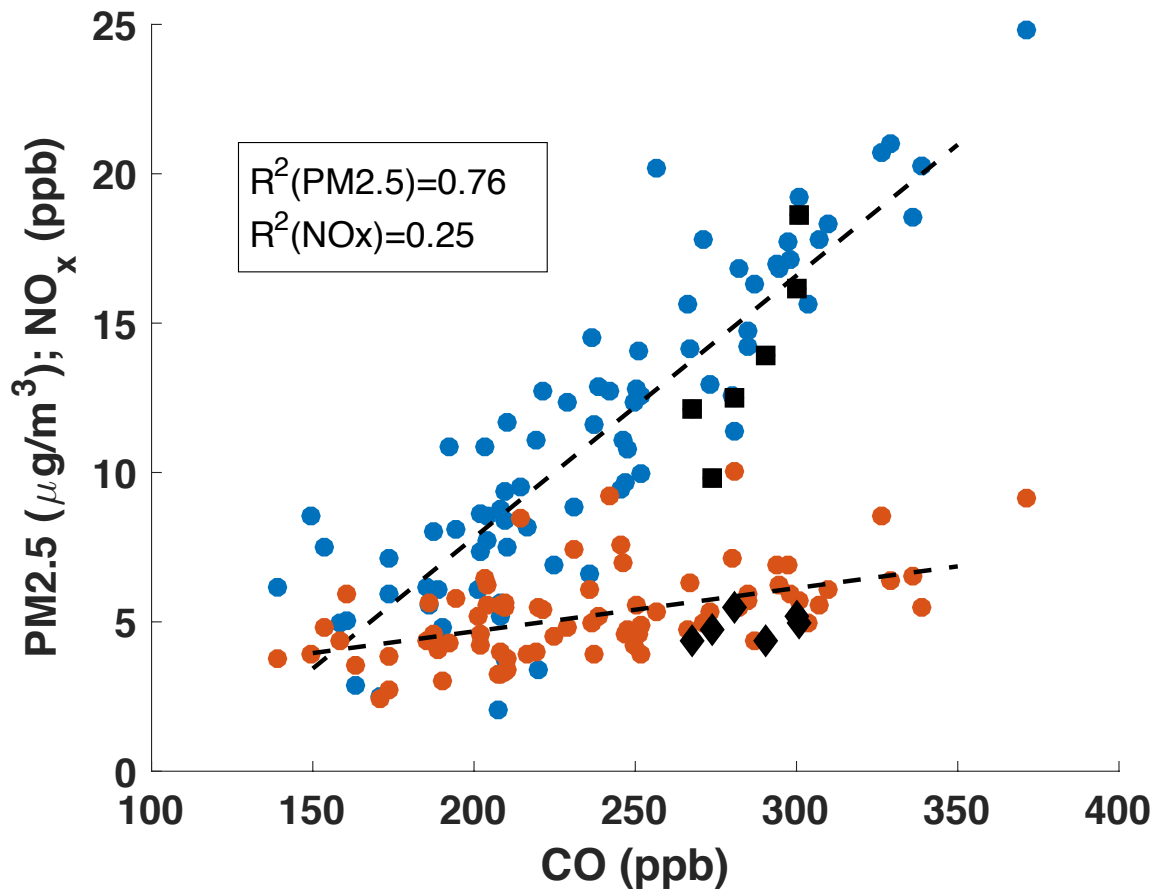
Figure 5. Data from CARB for Fresno-Garland and Clovis sites during Soberanes fire (07/22/16–10/12/16). Here we see a correlation between CO and PM2.5 (blue dots) but a weaker correlation between CO and NOₓ (orange dots). The black squares (PM2.5) and diamonds (NOₓ) are the six EPA flight dates.
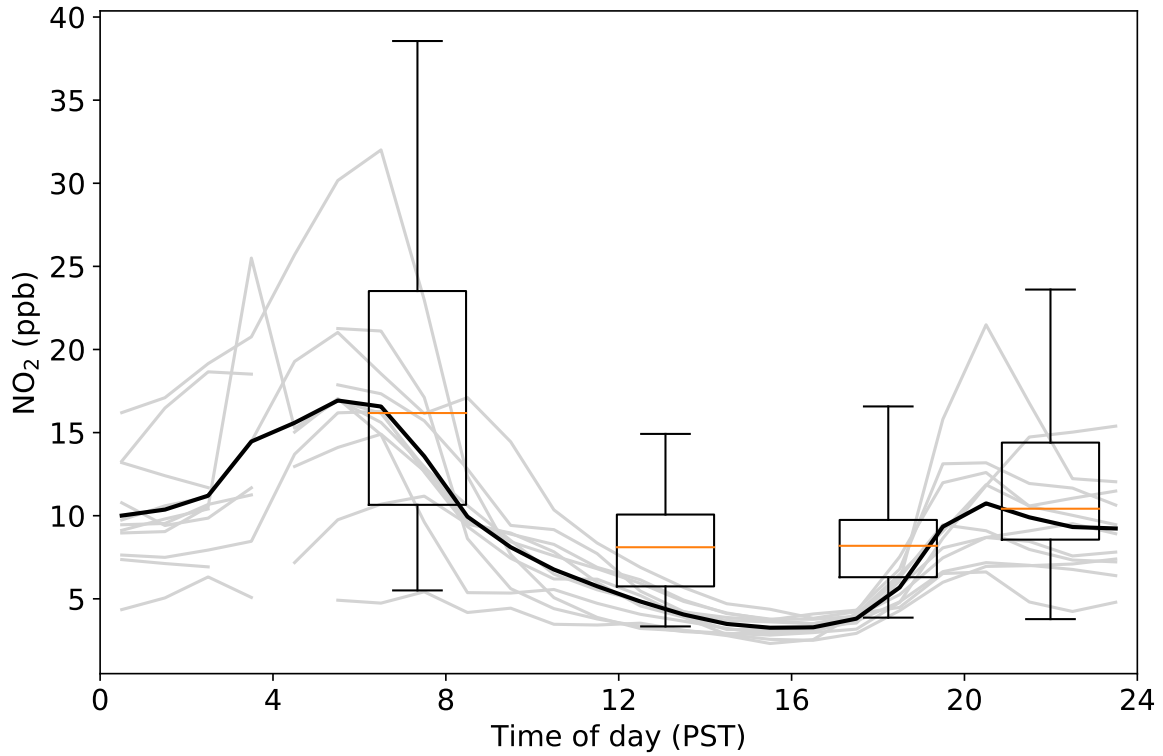
Figure 6. Box and whisker plots for flight data from RLO flights, and the grey lines are data from 11 CARB surface sites (see Figure 1). Statistics for box and whisker (lower adjacent, 25th percentile, median,75th percentile, upper adjacent): sunrise (-2.0, 10.7,16.2, 23.5, 42.7), afternoon (-0.3, 5.7, 8.1, 10.1, 16.5), evening (2.6, 6.3, 8.2, 9.7, 15), night (0.6, 8.6, 10.4, 14.4, 23.1).
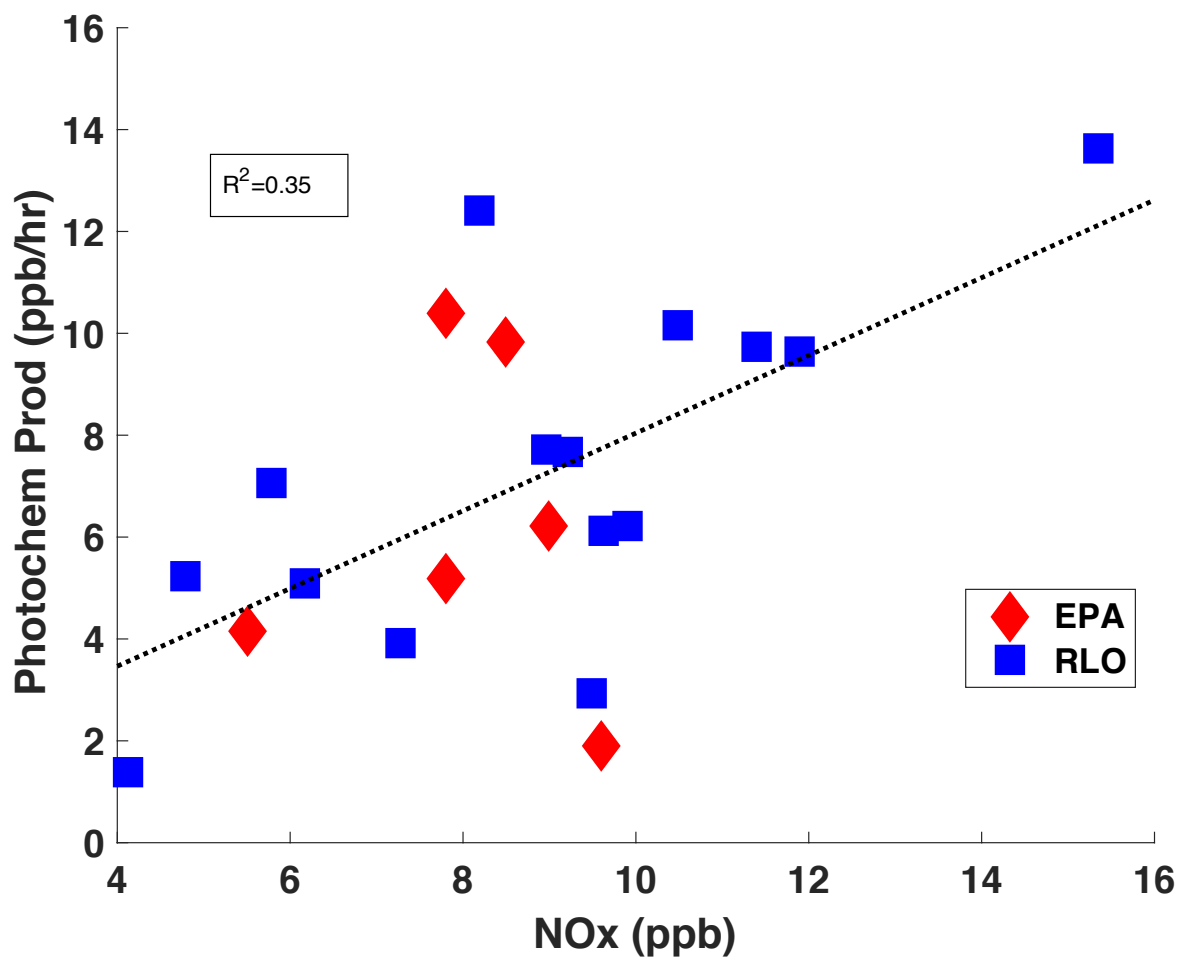
Figure 7. Correlation between photochemical production and NO$_x$ improved after including the additional 15 RLO flights. The correlation suggests that the flight region is in the NO$_x$-limited regime.
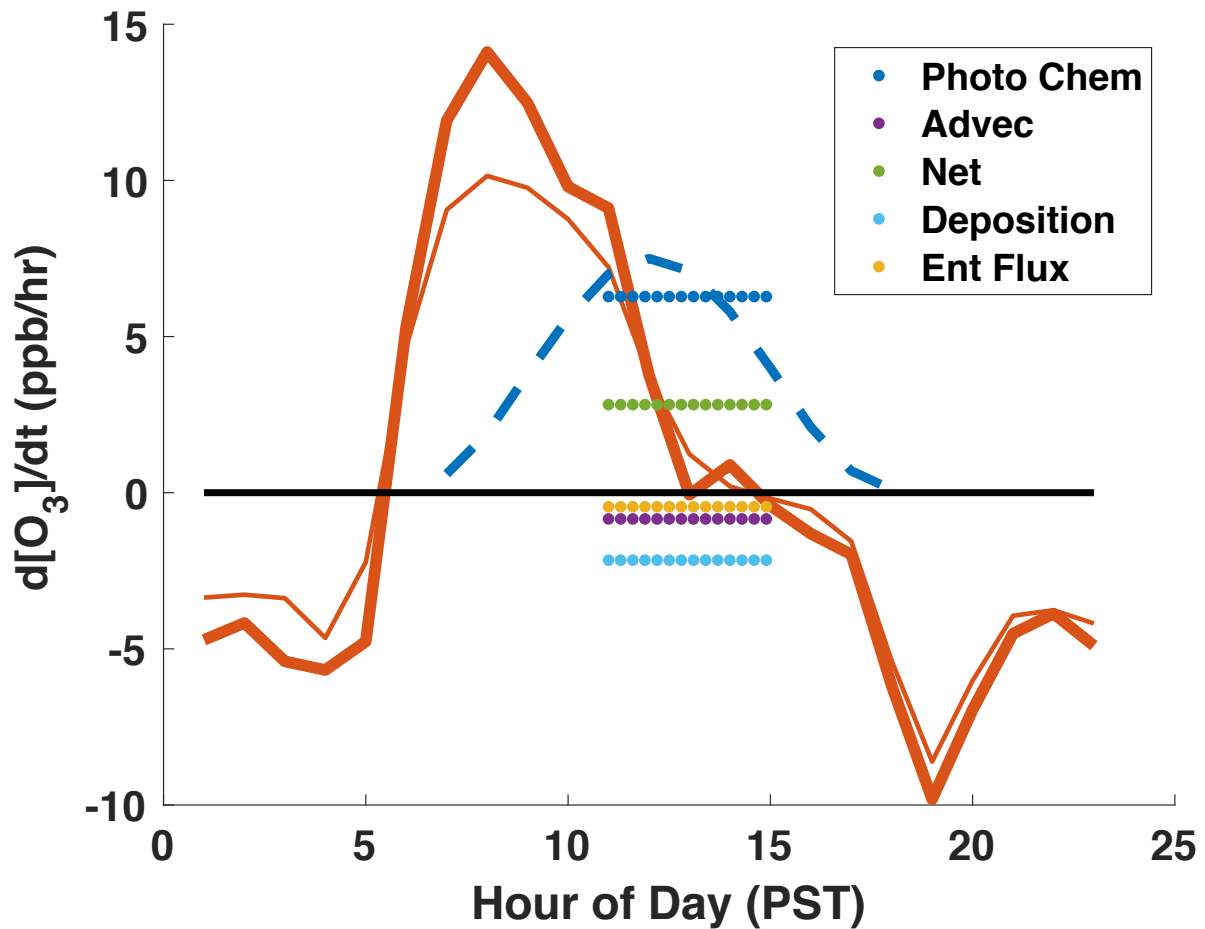
Figure 8. Thick orange line comes from CARB data from seven sites in the vicinity of the EPA flights (see Figure 1) for June, July, and August. The thinner orange line is from the six flight days themselves. Horizontal dotted lines show each respective averaged ozone budget term over the flight hours and the EPA flights. The rapid increase in ozone levels in the early morning corresponds to when the ABL entrains residual layer air. The graphic helps to visualize the breakdown of the O_3 budget during the flight hours in comparison to the time rate of change of O_3 observed by local surface stations.
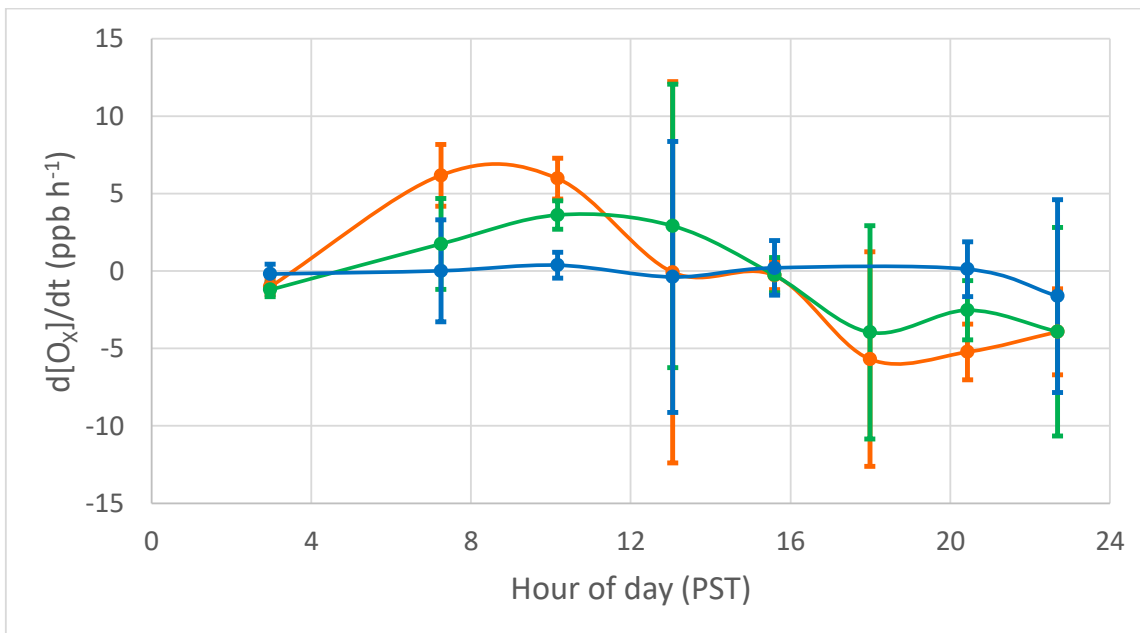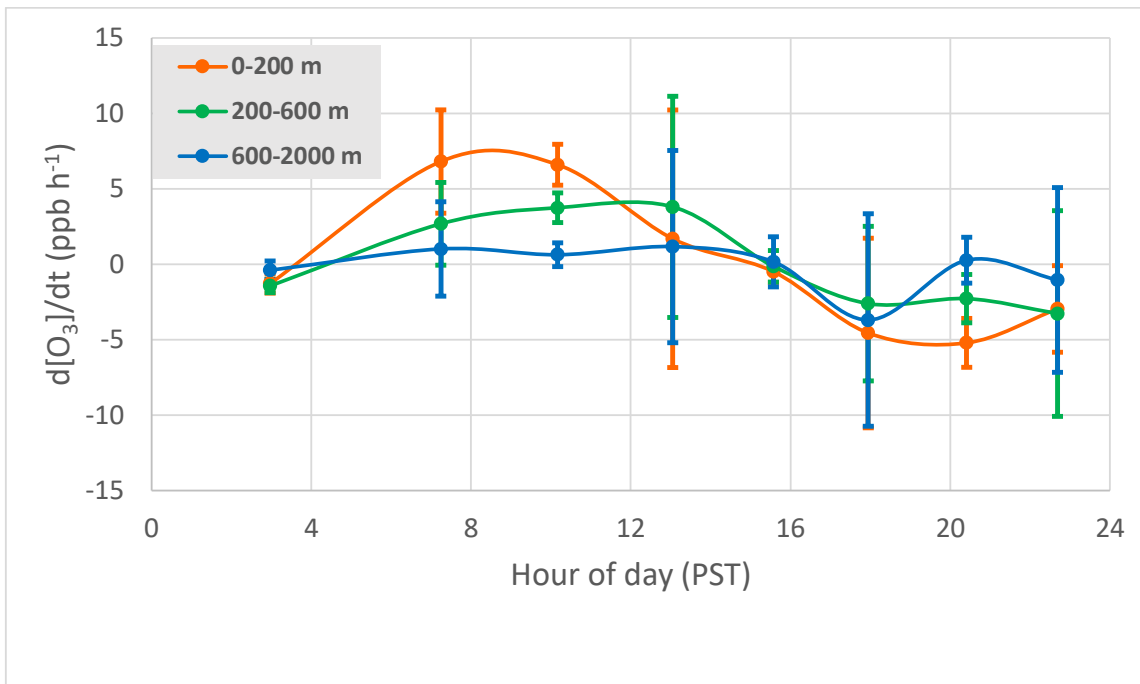
Figure 9. The average time rate of change of (a) O₃ and (b) Oₓ over a complete diurnal cycle. The curves are cubic polynomial interpolations between averaged data points from the RLO flights over each 2 hour measurement period and intervals in between flights. Data is binned into 3 altitude layers: the lower boundary layer 0-200 m, the upper boundary layer 200-600 m, and the buffer layer 600-2000 m. Vertical bars about each point represent one standard deviation of the 15 flight sequences.
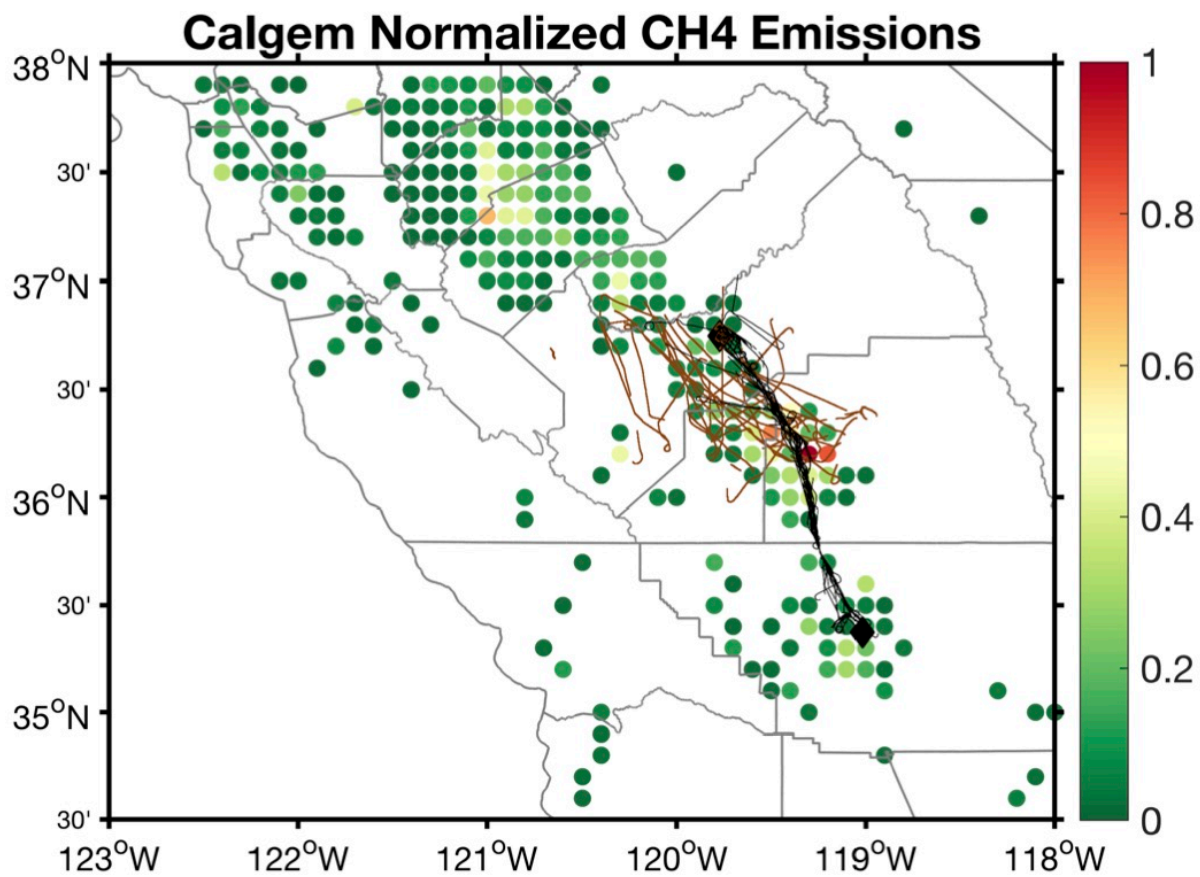
Figure 10. **Normalized CALGEM inventory emissions showing the distribution and relative magnitude of methane sources with flight tracks (EPA flights in brown and RLO flights in black) overlain. At the northern and southern ends of the RLO flights are black diamonds representing Fresno and Bakersfield, respectively.**
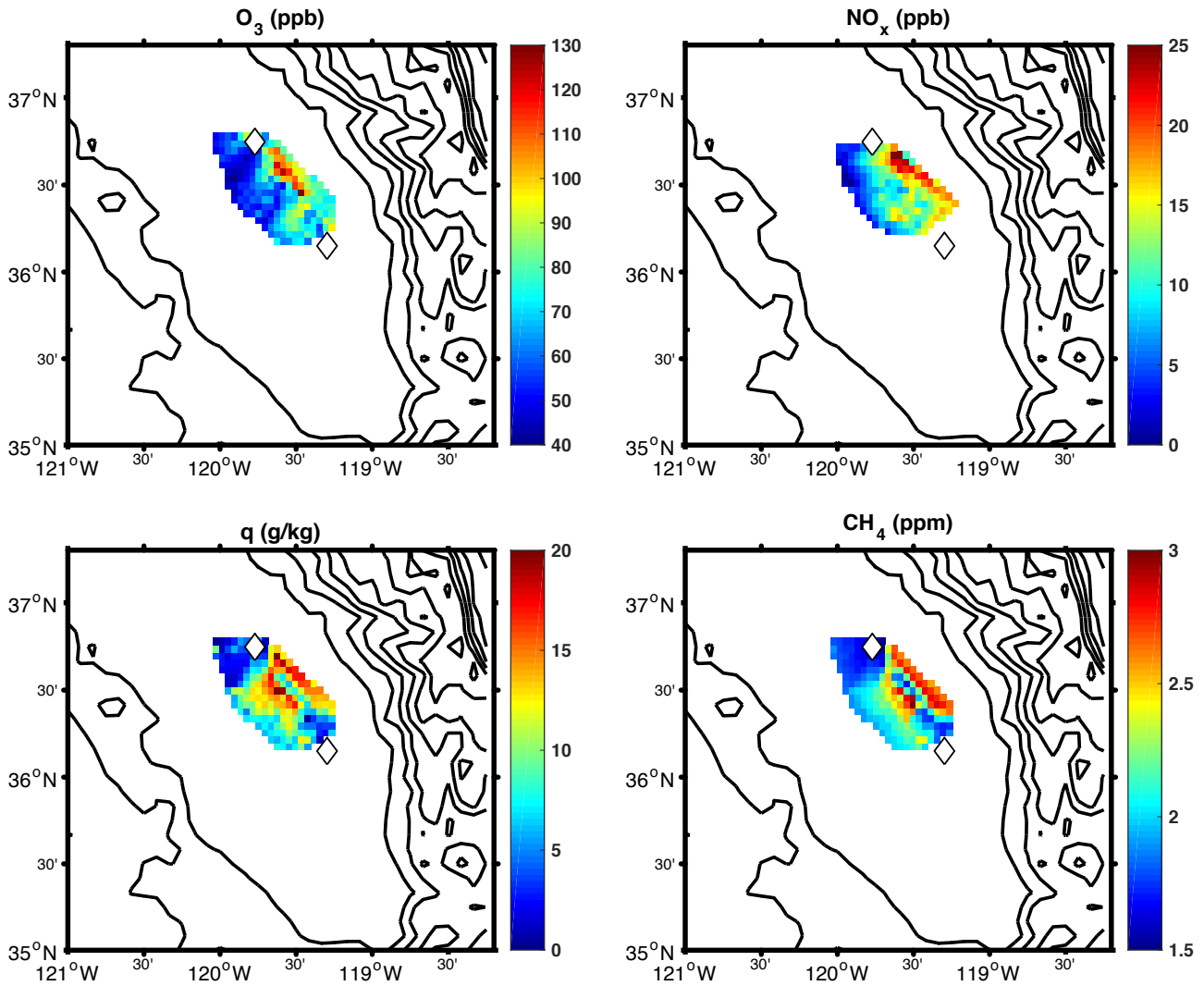
Figure 11. "Scalar Patchiness" plots derived from ABL flight data corrected to a common time and height stamp with linear interpolation between data points within the flight domain. White diamonds are Fresno at the north end and Visalia at the southern end. Data taken from July 27, 2016.
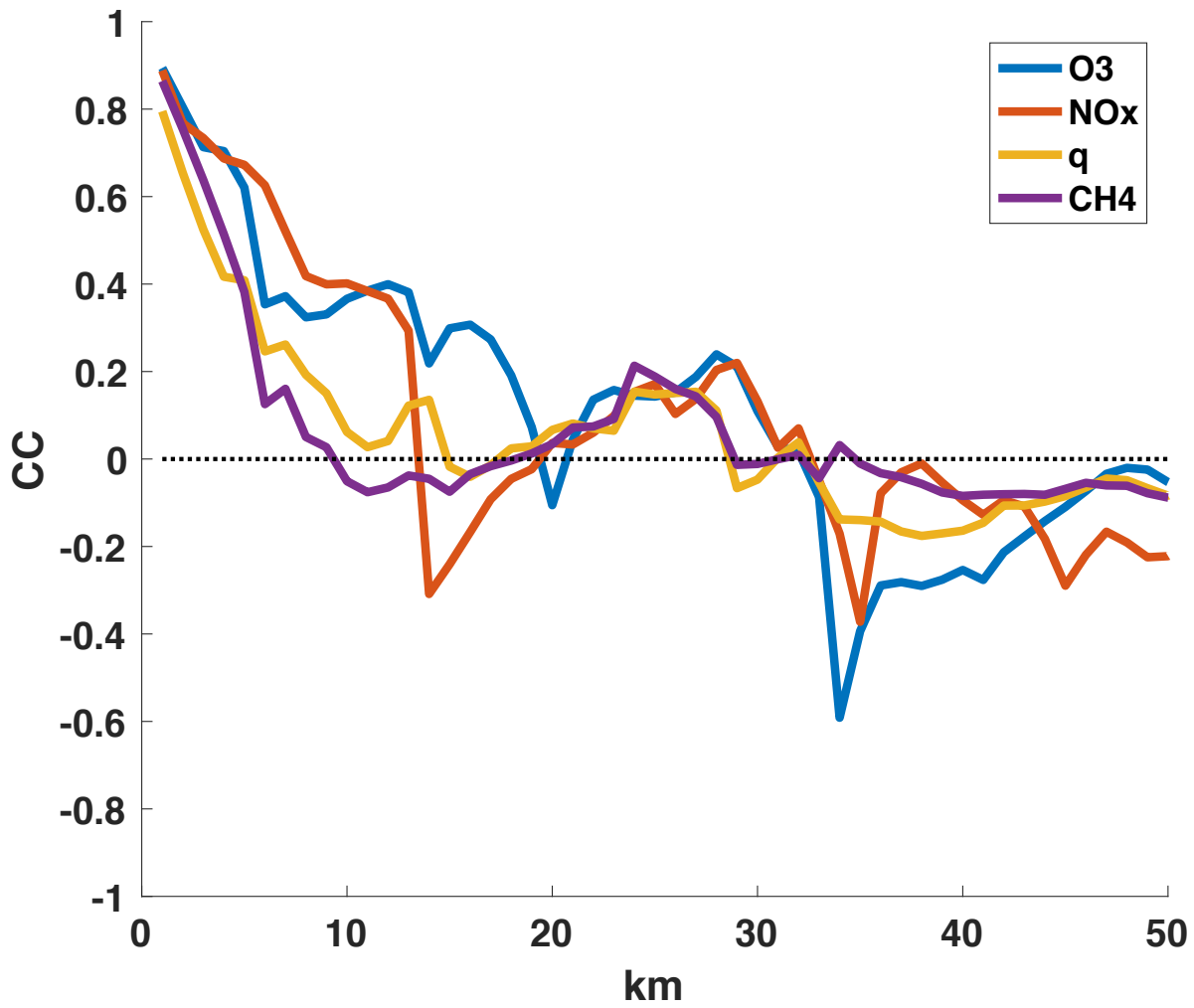
Figure 12. Spatial correlation plot corresponding to the patchiness plot from July 27, 2016. The y-axis shows the correlation coefficient (CC) and the x-axis shows the distance in kilometres for which the data has been correlated. 'q' signifies water vapor.